ERRATA

1. Page 25: ($\alpha, 3\pi\xi$) should read ($\alpha, 2\pi\xi$), and ($\alpha, 4\pi\xi$) should read ($\alpha, 3\pi\xi$).
2. Figure 7-5, page 20, and Figure 18-4, page 41, are interchanged.
3. Equation (2), page 13, is correct only if the incoming proton beam is polarized. For an unpolarized beam, W ($\theta_\gamma = \pi, \phi_\gamma, \phi_p$) is the sum of W^+ and W^- where the (+) and (-) superscript refers to spin "up" and spin "down", respectively. Each of the amplitudes "a" are then also designated by (+) and (-) superscripts. The in-plane angular correlation function is then given by

$$W = (a_1^2 - 2D + a_{-1}^2) + (a_2^2 - 2E + a_{-2}^2) + 4D\sin^2(\phi_\gamma - \epsilon_1) + 4E\sin^2 2(\phi_\gamma - \epsilon_2)$$

where $a_i^2 = (a_i^+)^2 + (a_i^-)^2$, etcetera,
and D, E, ϵ_1 and ϵ_2 are functions of the magnitude and phase of the "a's".
If we now set $S = a_1^2 + a_{-1}^2$ in equation (1), and $K = (a_1^2 - 2D + a_{-1}^2) + (a_2^2 - 2E + a_{-2}^2)$ then we obtain

$$a_2^2 + a_{-2}^2 = K + 2D + 2E - S$$

$$a_0^2 = 1 - S - (a_2^2 + a_{-2}^2)$$

These formulae, together with S (the spin flip), are the substate populations, and replace equations (3) through (10). This means that one cannot find population differences, and columns 7, 8, and 9 in Table 7-1 are incorrect. Columns 4, 5, and 6 are unaffected. Figure 7-6 is in error, as are the conclusions concerning polarization.

UNIVERSITY OF WASHINGTON

Department of Physics

Cyclotron Research

PROGRESS REPORT FOR YEAR ENDING JUNE 15, 1962

PROGRAM "A"--EXPERIMENTAL PHYSICS PROGRAM (CYCLOTRON)

UNDER

U.S. ATOMIC ENERGY COMMISSION CONTRACT A.T. (45-1)-1388

PREFACE

This report reviews the research and technical developments conducted at the 60-inch cyclotron at the University of Washington during the year ending June 15, 1962.

Many investigations described in this report have continued to advance experimental work on topics described in several earlier reports. Notable among these are the studies of alpha particle scattering from light elements; the investigation of symmetry axis behavior in (α, γ) angular correlations; the various studies of nuclear fission; and the many experiments relating to compound nuclear reactions. In addition to these, several new areas of research are reported: among them are the determination from (p, γ) angular correlations of spin substate amplitudes in inelastic proton scattering; the use of time-of-flight techniques to detect very low energy charged particles from compound nuclear reactions; and the study of two nucleon stripping and pickup reactions. A more comprehensive list of the topics studied is given in the Table of Contents.

Research at this laboratory is performed by the faculty and graduate students of the Departments of Physics and Chemistry of the University of Washington. Support for this project is provided by the State of Washington, the U.S. Atomic Energy Commission, and the National Science Foundation*.

Except for minor changes, the arrangement of this report follows the pattern used in previous years. The sections are numbered consecutively through the report; each table and figure is assigned the number of the section to which it pertains. As has been our practice, the names of investigators listed at the end of each section are given in strict alphabetical order.

---

*The National Science Foundation has provided funds for the purchase of the three-stage Tandem Van de Graaff accelerator and, in part, for the building to house the new accelerator.

TABLE OF CONTENTS

I. BETA AND GAMMA RAY SPECTROSCOPY

1. Principal Decay Mode of C^{10}

The study of the higher energy positron branch from C^{10} with the toroidal spectrometer[1] has been completed. Our final value for the end-point energy after several improvements and careful checking of the experimental procedure, is 1.865 ± 0.015 Mev. A Fermi-Kurie plot is shown in Fig. 1-1.

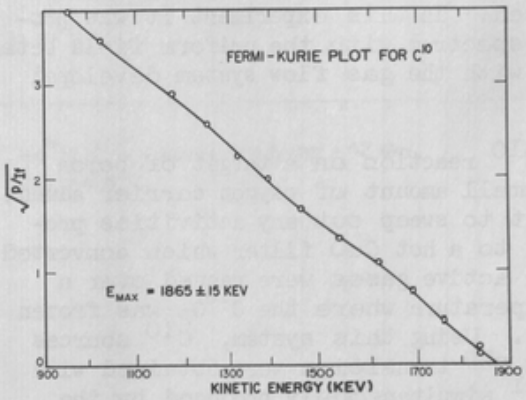

Figure 1-1

Fermi-Kurie plot for the 1.865 Mev transition from C^{10}.

The toroidal spectrometer has been discussed in previous progress reports.[2] We describe here only recent changes in the detectors and the B^{10} targets. A scintillation counter has been installed as the detector of the spectrometer. Since it records all the particles passing through the ring baffle, the counting statistics remained essentially the same with the new, thinner targets as with the smaller Geiger counter and the old B^{10} pressed powder targets. The new targets were formed by deposition of a 97% B^{10} slurry on a 1/4 mil Mylar backing. The accuracy of the source normalization provided by the monitor was improved by mounting this counter closer to the source.

Many possible sources of error in the end-point determination have been investigated. Any magnetic interaction between the toroidal spectrometer and the scintillation counters was demonstrated to be insignificant regardless of their relative proximity. A counting rate effect in the monitor counter has been considered and experimentally found to be negligible.

The quality of our C^{10} sources was examined. We found that the major radioactive contaminant is C^{11} produced from the 3% B^{11} impurity in the target. With our usual monitor counter system and the half-life unit developed by Penning[3] we proved that a single nuclear species, presumably C^{10}, had been investigated. Its half-life was found to be 19.27 ± 0.08 seconds. As a result of this half-life measurement we re-examined the high-energy tails observed in our earlier spectra.[2] We found that they were due to gamma rays produced from the C^{10} source. Their effect was essentially removed from our spectra by additional lead shielding around the detector of the spectrometer and an analysis of the dependence of this background on the spectrometer current. (F. J. Bartis and F. H. Schmidt).

1 We have accepted the simpler and more common designation of "toroidal spectrometer" in place of the name "iron-free orange spectrometer" used in previous reports.
2 Cyclotron Research, University of Washington (1961) p.2; (1959) p.7; (1957) p.2.
3. John R. Penning, Jr., Thesis, University of Washington, 1955 (unpublished).

2. Decay Scheme of C^{10}

In a previous report[1] an experiment to determine the branching ratio for the $0^+ \rightarrow 0^+$ transition of C^{10} was discussed. In this experiment it was proposed to make a careful study of the C^{10} spectrum with the uniform field beta-ray spectrometer using a source produced with the gas flow system developed for studying O^{14}.

C^{10} was prepared by the B^{10} (p, n) C^{10} reaction on a target of boron powder enriched in B^{10}. Helium, with a small amount of oxygen carrier added, was passed continuously through the target to sweep out any activities produced. The active gases were then passed to a hot CuO filter which converted the C^{10} activity to $C^{10}O_2$. Finally, the active gases were passed over a copper button held at liquid nitrogen temperature where the $C^{10}O_2$ was frozen out to make a source for the spectrometer. Using this system, C^{10} sources of adequate strength to study the 1.8 Mev C^{10} transition were obtained with no difficulty. However, the amount of C^{11} simultaneously produced by the (p, n) reaction on the residual B^{11} in the target was so large as to severely limit the accuracy of the gamma-ray monitoring system used. This, along with a much smaller impurity of N^{13} in the target produced by the reaction O^{16} (p, α) N^{13} on the oxygen carrier, made it impossible to obtain reliable data on the C^{10} spectrum shape near the 1.1 Mev end point for the $0^+ \rightarrow 0^+$ transition. For these reasons this experiment has been discontinued. (J. B. Gerhart and G. S. Sidhu).

1 Cyclotron Research, University of Washington (1960) p. 4.

3. 4.1 Mev Positron Spectrum of O^{14}.

The experiment discussed in earlier reports[1] to determine the spectrum shape of the 4.1 Mev transition from O^{14} is being continued. In this case the 2.3 Mev gamma ray following the O^{14} decay has sufficient energy that, unlike the C^{10} gamma rays discussed in Sec. 2 above, it can be used to monitor the O^{14} source activity accurately. At the present time, extensive studies of background and stability are being made. The experiment should be concluded in the coming year. (J. B. Gerhart and G. S. Sidhu).

1 Cyclotron Research, University of Washington (1961), p. 2; (1959), p. 5.

II. NUCLEAR SCATTERING AND CORRELATIONS OF SCATTERED PARTICLES WITH GAMMA RAYS

4. Inelastic Scattering of Alpha Particles

(1) Scattering by Mg^{24}. A typical pulse height spectrum for particles from the alpha particle bombardment of Mg^{24} is shown in Fig. 4-1. No strongly excited levels were observed between Q = -4.2 Mev and -6.0 Mev for scattering angles below 60° (c.m.). The observed inhibition of the (α, α') reaction exciting the nucleus to the level at 5.22 Mev is of particular significance in view of the presumable unnatural parity[1] (3^+) of the level.

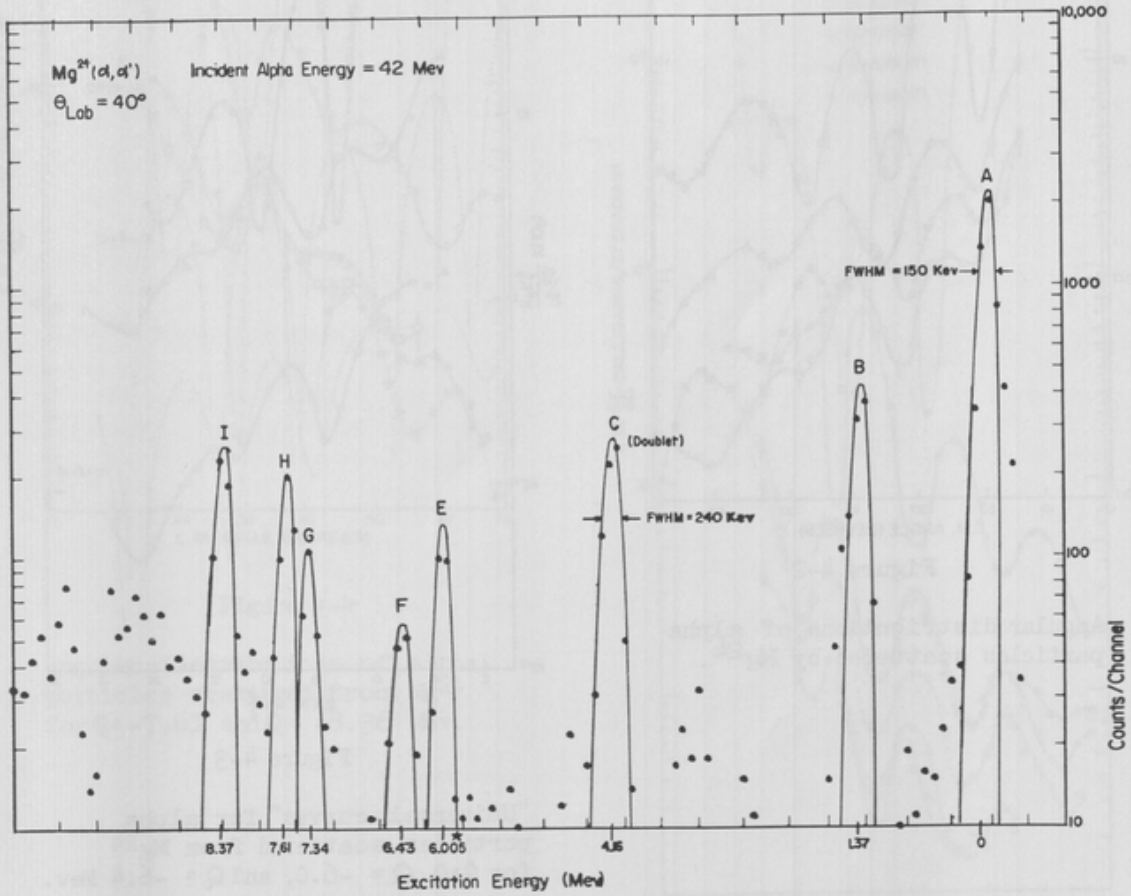

Figure 4-1

Pulse height spectrum of particles from the alpha particle bombardment of Mg^{24}.

The angular distributions corresponding to some of the strongly excited levels in Mg^{24} are shown in Fig. 4-2. Consideration of curve C for the doublet at Q = -4.16 Mev suggests that the 2^+ component of this doublet at Q = -4.23 Mev[2] may represent a vibrational collective excitation of the presumably deformed Mg^{24} nuclear surface.

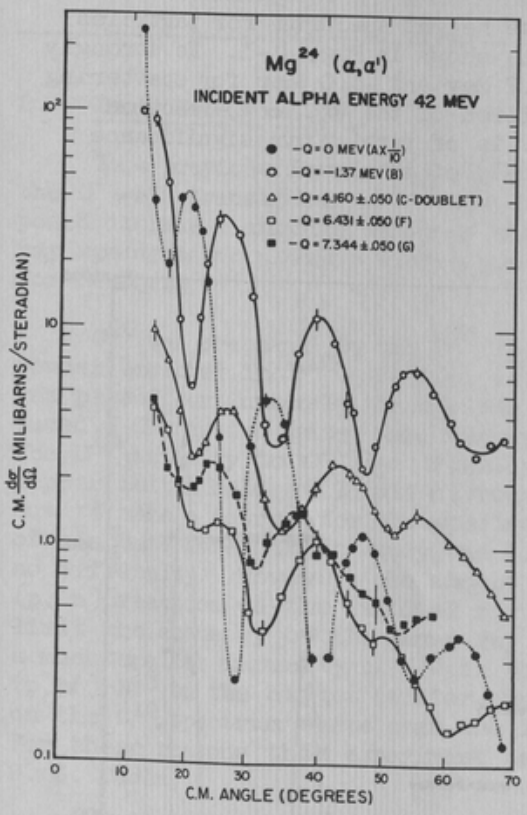

Figure 4-2

Angular distributions of alpha particles scattered by Mg^{24}.

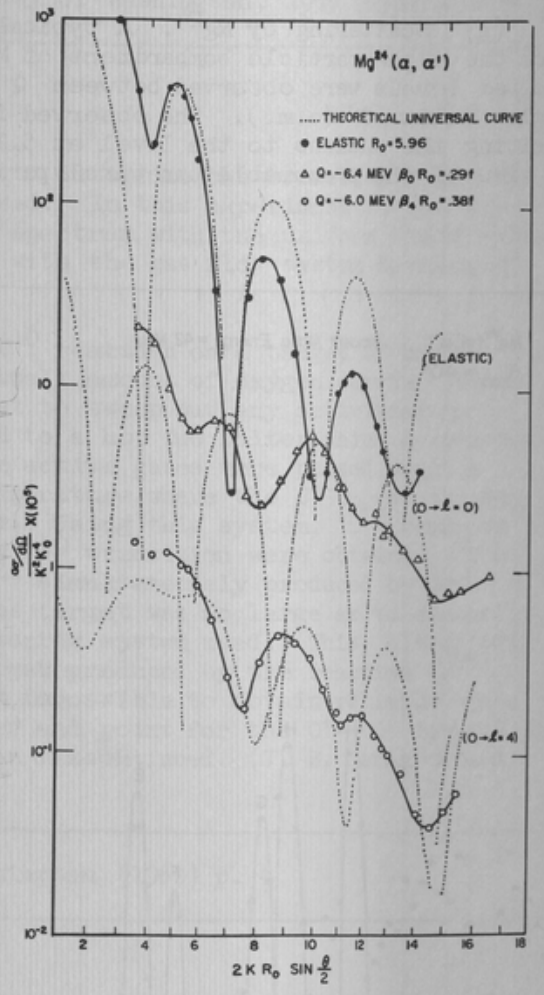

Figure 4-3

"Universal curves" for alpha particles scattered from Mg^{24} for Q=0, Q= -6.0, and Q= -6.4 Mev.

"Universal Curves" $(\frac{d\sigma}{d\Omega}/k^2R_o^4$ vs. $2kR \sin \theta/2)$ for scattering with Q = 0, Q = -6.0, and Q = -6.4 Mev are shown in Fig. 4-3. The dotted curves represent the predictions of the Fraunhofer formulas[3] of the inelastic diffraction model for the elastic and the inelastic (α, α') reactions involving $\ell = 4$ and

ℓ = 0 single phonon collective vibrations. In the angular distributions for the 6.0 and 6.4 Mev levels, the absence of the features expected for the double excitation process and the fair agreement with the Fraunhofer predictions suggest that the levels at 6.0 and 6.4 Mev may represent ℓ = 4 and ℓ = 0 single phonon collective vibrations, respectively.

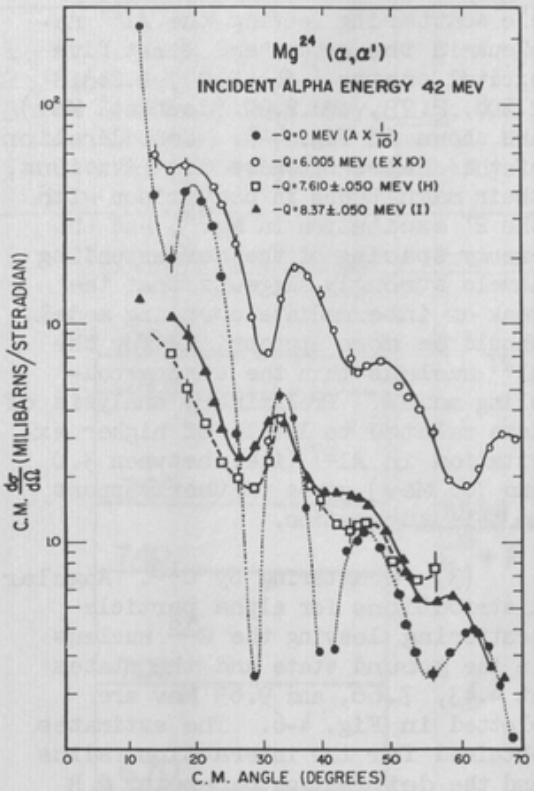

Figure 4-4

Angular distributions of alpha particles scattered from Mg^{24} for Q = -7.61 and Q = -8.36 Mev.

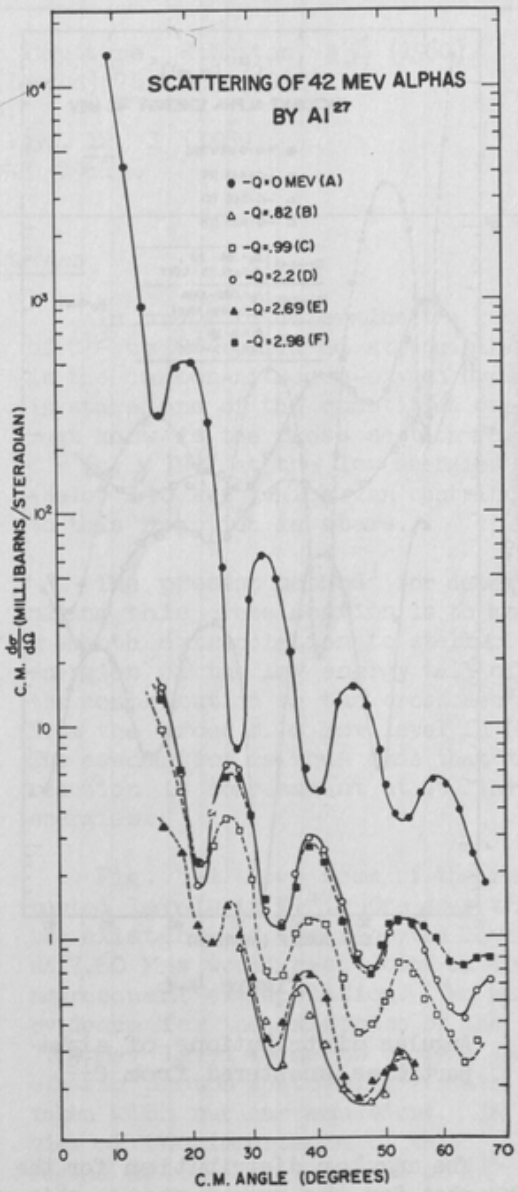

Figure 4-5

Angular distributions of alpha particles scattered from Al^{27}.

The angular distributions corresponding to the 7.61 and 8.36 Mev levels are shown in Fig. 4-4. The curves are quite similar in shape and both are in phase with the elastic angular distribution. This suggests the two levels may represent octupole excitations of the Mg^{24} nucleus.

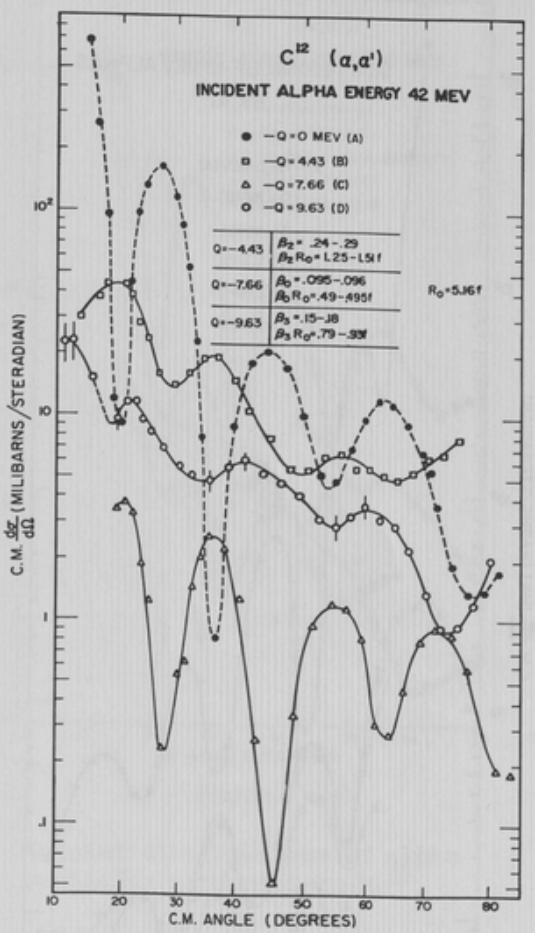

Figure 4-6

Angular distributions of alpha particles scattered from C^{12}.

(2) Scattering by Al^{27}. Angular distributions for alpha particle scattering leaving the Al^{27} nucleus in the ground and first five excited states ($-Q = 0.84$, 1.013, 2.208, 2.73, and 2.99 (doublet) Mev) are shown in Fig. 4-5. Consideration of the shapes of these distributions, their magnitudes in comparison with the 2^+ excitation in Mg^{24}, and the energy spacing of the corresponding levels strongly suggests that the weak or intermediate coupling model should be more appropriate for the Al^{27} nucleus than the strong coupling model. Preliminary analysis of data related to levels of higher excitation in Al^{27} (i.e. between 3.0 and 7.5 Mev) gives further support to this suggestion.

(3) Scattering by C^{12}. Angular distributions for alpha particle scattering leaving the C^{12} nucleus in the ground state and the states at 4.43, 7.66, and 9.63 Mev are plotted in Fig. 4-6. The estimates obtained for the interaction radius and the deformation parameter $\beta_\ell R$ corresponding to the excitation of the nucleus to the 4.43 Mev (2^+) and 7.66 Mev (0^+) states are in agreement with other estimates[3] from previous experiments[4]. The peak-to-valley ratios, however, are distinctly higher and the detailed agreement with the inelastic diffraction predictions is more pronounced in the present experiments.

The angular distribution for the 9.6 Mev state is fairly closely in phase with that for the ground state; this supports the 3^- assignment of this level indicated by other experiments[5].

(4) Scattering by Mg^{24} and Mg^{26}. Elastic and inelastic scattering of alpha particles by enriched targets of Mg^{25} and Mg^{26} has been observed in the angular range 10° to 64° (lab.). Analysis is incomplete, but six to ten excited states between 0 and 8 Mev are clearly discernible at most angles of observation in each case. Further work at both smaller and larger angles is planned. (G. W. Farwell, I. Naqib, and D. Shreve).

---

1 H. E. Gove, Proc. Intern. Conf. Nuclear Structure, Kingston, 438 (1960).
2 Hinds and Middleton, Proc. Phys. Soc. (London) 76, 553 (1960).
3 J. S. Blair, Phys. Rev. 115, 928 (1959).
4 A. I. Yavin and G. W. Farwell, Nuclear Phys. 12, 1 (1959).
5 Richard R. Carlson, Nuclear Phys. 28, 443 (1961).

---

5. Inelastic Scattering of Protons by Nitrogen

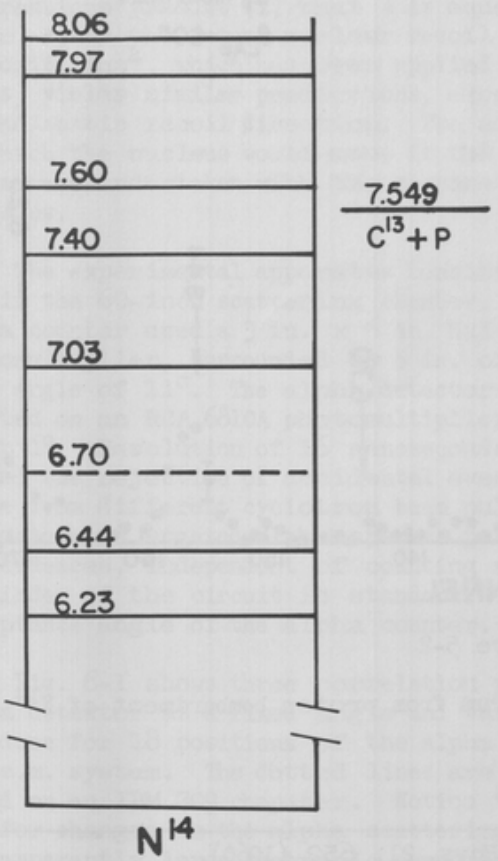

Figure 5-1

Portion of the level scheme of N^{14}.

In order to determine the ratio of C^{12} to C^{13} produced at equilibrium in the carbon-nitrogen-oxygen cycle in stars, one of the quantities one must know is the cross section for $C^{13}(p,\gamma)N^{14}$ at the low energies (below 100 kev) which can contribute to this reaction in stars.

The present method[1] for determining this cross section is to make a smooth extrapolation to stellar energies of the low energy tail of the contribution to the cross section from the broad 8.06 Mev level in N^{14}. The assumption is thus made that the reaction is nonresonant at stellar energies.

Fig. 5-1 shows some of the reported levels in N^{14}. One sees that the existence of the reported level at 7.60 Mev would cast doubt on the nonresonant extrapolation. The main evidence for the existence of the 7.60 Mev level seems to be from inelastic proton scattering[2,3] data taken with nuclear emulsions. In view of the importance of this region of the level scheme of N^{14} for astrophysics, it was decided to use the 10.5-Mev proton beam from the

University of Washington cyclotron to investigate N^{14} in the appropriate region of excitation by means of inelastic proton scattering.

The gas cell described in Sec. 25, filled with commercial nitrogen, serves as a target. A solid state detector capable of stopping 10 Mev protons is used to detect the scattered protons, and the pulses from the detector are displayed on a 512-channel pulse height analyzer. To-date, only a small amount of data has been taken; however, it can be stated that no evidence for a strongly excited state near 7.60 Mev excitation in N^{14} has been found. This is in contrast to the 9.5 Mev data reported by Burge and Prowse[3]. Fig. 5-2 shows a low energy section of the scattered proton spectrum taken here at a laboratory angle of 60°. Work on this experiment is being continued. (R. E. Brown).

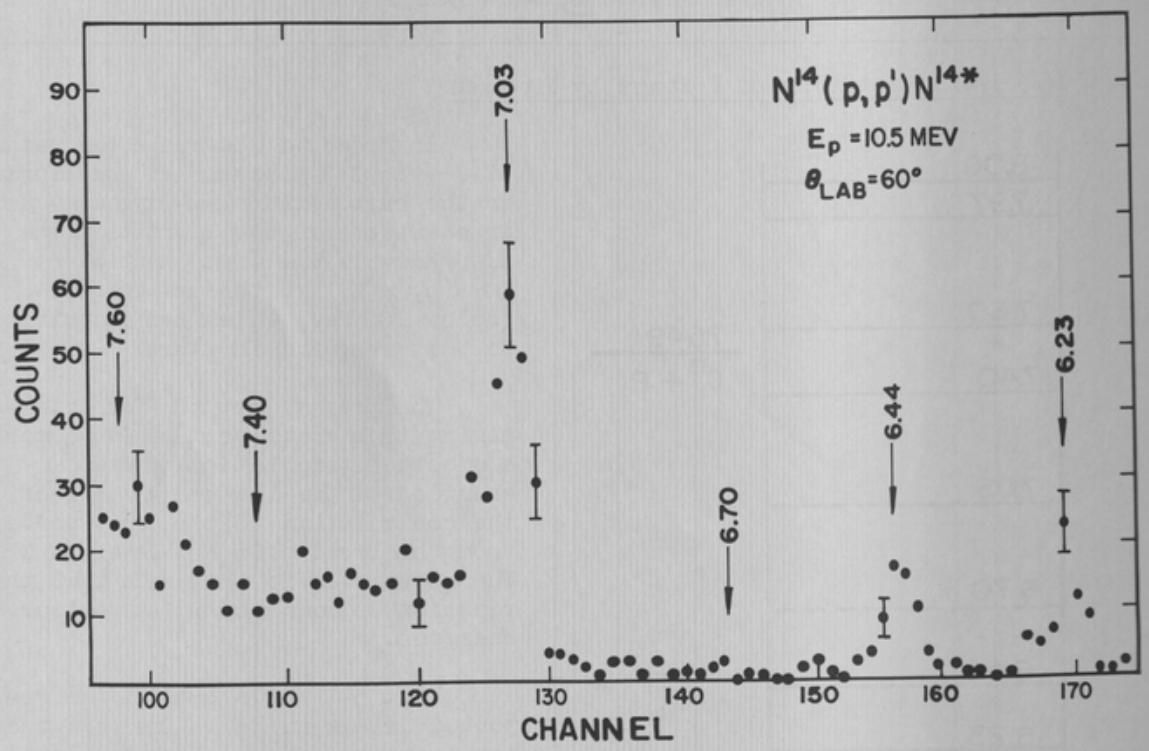

Figure 5-2

Low energy portion of the proton spectrum from proton bombardment of N^{14}.

1 D. F. Hebbard and J. L. Vogl, Nuclear Phys. 21, 652 (1960).
2 F. Ajzenberg-Selove and T. Lauritsen, Nuclear Phys. 11, 1 (1959).
3 E. J. Burge and D. J. Prowse, Phil. Mag. 1, 912 (1956).

6. Symmetry Axis Behavior of (α,γ) Correlations in C^{12} $(\alpha,\alpha'\gamma)$ Reactions

The measurements of (α,γ) angular correlations in $C^{12}(\alpha,\alpha'\gamma)$ reported earlier[1] have been continued. Coincidence counting was done between the inelastically scattered alpha particle and the de-excitation gamma ray from the first excited state of C^{12}. A correlation pattern was obtained by placing the alpha-particle detector in a fixed position and rotating the gamma detector about the target in the scattering plane. Correlation patterns were taken in this manner for closely spaced alpha scattering angles in the forward direction. This permitted us to observe the variation of the correlation parameters as a function of the alpha scattering angle. All pertinent directions lie in the scattering plane and all angles are measured with respect to the incident beam direction. The most general form for the correlation function, in the scattering plane, for such a $0^+ \rightarrow 2^+ \rightarrow 0^+$ transition is given by the 5 parameter function $W(\theta) = A + B \sin^2 2(\theta - \theta_o) + C \sin^2 (\theta - \theta_1)$. For particles of zero spin, taking into account conservation of parity and symmetry about the scattering plane[2], this formula reduces to $W(\theta) = A + B \sin^2 2(\theta - \theta_o)$. This, then, is the most general formula for the alpha particle. Plane-wave Born theories[3] of direct interactions predict (1) that A is equal to zero and (2) that θ_o lies along θ_R where θ_R is the actual nuclear recoil direction. The less sweeping adiabatic approximation[4], which has been applied successfully in fitting angular distributions, yields similar predictions, except that now the symmetry axis lies along the adiabatic recoil direction. The adiabatic recoil direction is the direction in which the nucleus would move if the excitation energy were zero. Our measurements were undertaken with the purpose of testing these two rather simple theories.

The experimental apparatus consisted of the two movable detectors, located within the 60-inch scattering chamber, and their associated electronics. The gamma counter used a 3 in. x 6 in. NaI (Tl) crystal mounted on an RCA 6810A photomultiplier, surrounded by 5 in. of lead shielding, and had a half acceptance angle of 11°. The alpha detector used a 40 mil NaI (Tl) crystal, also mounted on an RCA 6810A photomultiplier, and had a half acceptance angle of about 1°. Resolution of 16 nanoseconds in the fast coincidence circuit permitted the rejection of accidental events in which the alpha and gamma counts arose from different cyclotron beam pulses. Simultaneous observation of both the gated and ungated alpha spectra permitted quick evaluation of accidental coincidences, independent of counting rate fluctuations (see Sec. 7). The remainder of the circuit is standard. Crucial to our experiment is the small acceptance angle of the alpha counter.

Fig. 6-1 shows three correlation patterns that were taken by setting the alpha detector at a fixed angle and varying the gamma counter position. This was done for 18 positions of the alpha counter, ranging from 13.6° to 55.8° in the c.m. system. The dotted lines are least squares fits to the data, computed on an IBM 709 computer. Notice the large change in the symmetry angle, θ_o, for changes in the alpha scattering angle of less than 11°. Notice also the apparently large isotropic component at $\theta_\alpha = 32.4°$.

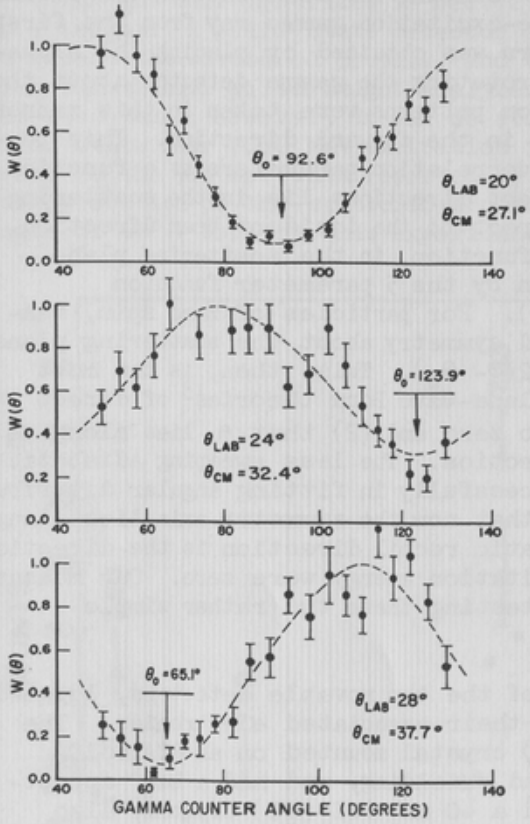

Figure 6-1

Selected (α, γ) angular correlations for C^{12} $(\alpha,\alpha'\gamma)C^{12}$.

In Fig. 6-2 the symmetry angle, θ_o, is plotted as a function of the alpha scattering angle. Because the general correlation function $W(\theta) = A + B \sin^2 2(\theta - \theta_o)$ repeats every 90^o in θ, the points plotted as open circles are duplicates of points plotted already at $\theta + 90^o$. This was done to show that there is no way to determine which point is more basic. The points plotted as crosses are data of Shook[5]. The solid lines are the loci upon which the data points are expected to fall using the plane-wave Born approximation and the adiabatic approximation. Our results coincide with neither of these simple theories at points away from maxima of the inelastic differential cross section. In fact, the data show a rotation of the symmetry axis through an angle of about 90^o relative to the predictions of these theories. These simple theories clearly are not capable of explaining the complex behavior of the symmetry axis observed here.

Figure 6-3 shows the ratio A/B, also plotted as a function of the alpha scattering angle. The simple theories predict that this ratio should be zero. Because of the large uncertainties, this possibility cannot be ruled out. The uncertainties are particularly large near minima of the differential cross section. These are the points where θ_o rotates most rapidly as a function of the alpha scattering angle, giving rise to large finite geometry corrections. In fact, an alpha acceptance angle of 4^o would be equivalent to a gamma acceptance angle of about 60^o, which would virtually destroy the correlation pattern. We have just completed an additional measurement of the correlation function at $\theta_\alpha = 32.4^o$ with an even smaller alpha acceptance angle. Preliminary evaluation of this measurement yields an A/B ratio of 0.33 ± 0.10, significantly different from zero in this case.

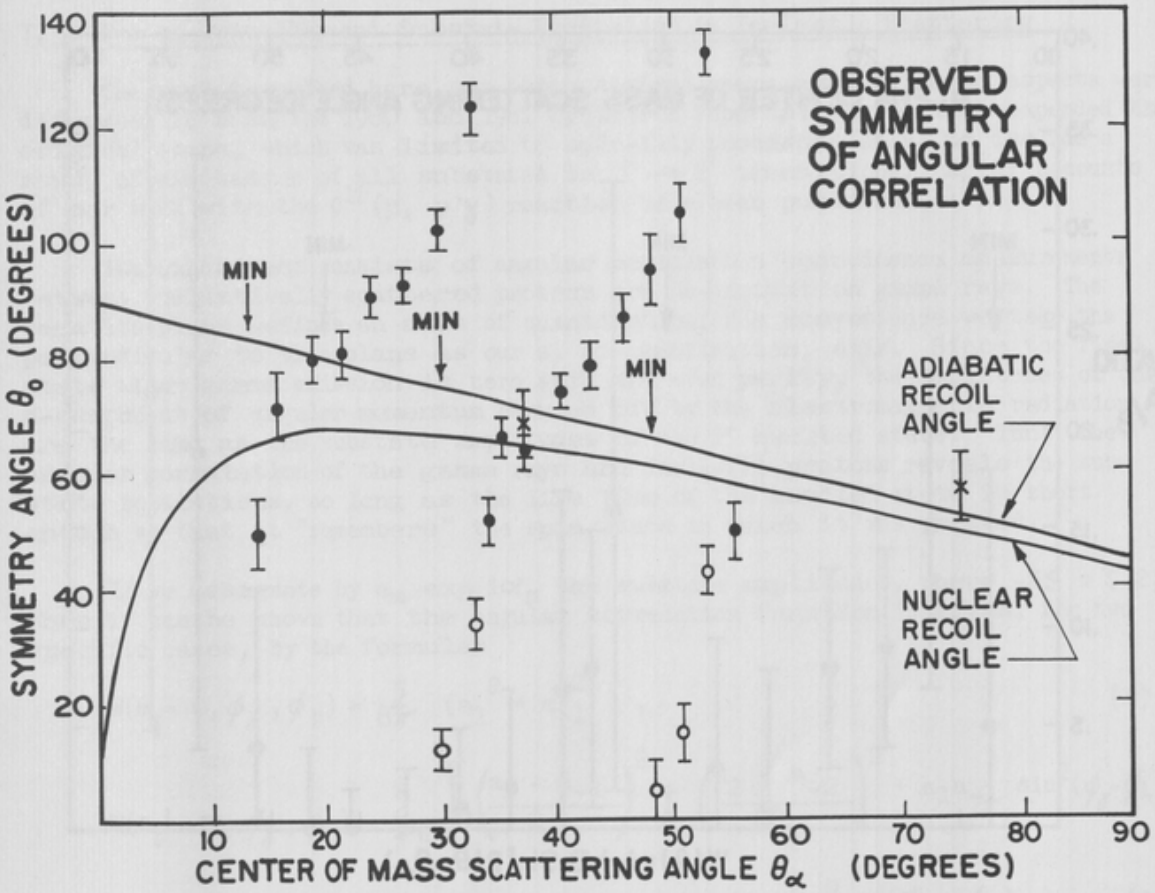

Figure 6-2

Symmetry angle vs. alpha particle scattering angle.

Recently Satchler[6] has performed distorted-wave Born approximation calculations, which yield predictions in very good qualitative agreement with our experimental results. No physical explanation of these results has yet been achieved. A preliminary report of our experimental results has been published[7]. (D. L. Hendrie and D. K. McDaniels).

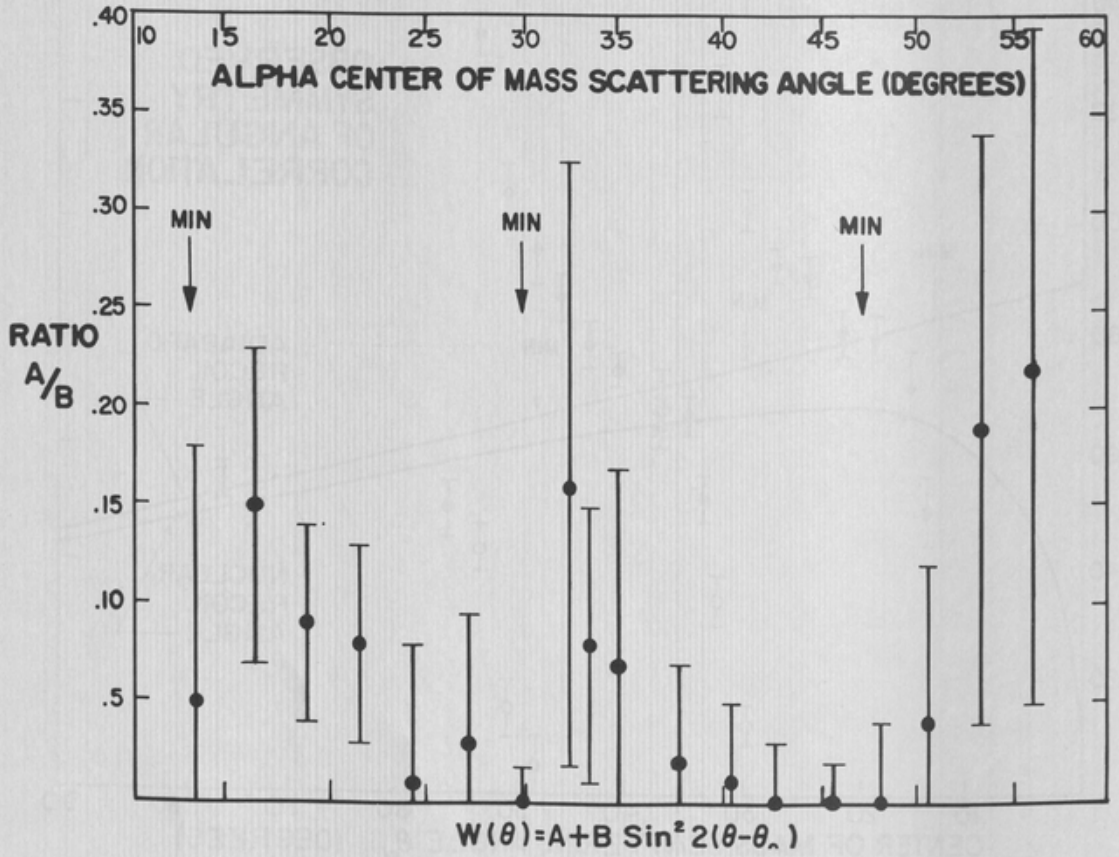

Figure 6-3

(A/B) vs. alpha particle scattering angle.

1 Cyclotron Research, University of Washington (1961) p. 7.
2 A. Bohr, Nuc. Phys. 10, 486 (1959).
3 G. R. Satchler, Proc. Phys. Soc. (London) A68, 1037 (1955).
4 J. S. Blair and L. Wilets, Phys. Rev. 121, 1493 (1961).
5 G. B. Shook, Phys. Rev. 114, 310 (1959).
6 Private communication.
7 D. L. Hendrie and D. K. McDaniels, Bull. Am. Phys. Soc. 7, 270 (1962).

7. Proton Spin-Flip and Substate Excitation in Inelastic Scattering

The work described here was begun several years ago, and some aspects were discussed in both the 1960 and 1961 Cyclotron Reports.[1,2] We have expanded the original scope, which was limited to spin-flip processes only, to include a study of excitation of all substates in $0^+ \rightarrow 2^+$ transitions. Brief accounts of our work with the $C^{12}(p, p'\gamma)$ reaction have been published.[3,4]

The experiment consists of angular correlation coincidence measurements between inelastically scattered protons and de-excitation gamma rays. The reaction plane defines an axis of quantization; for convenience we take the perpendicular to this plane as our z, or quantization, axis. Since the final state after gamma emission is zero spin and even parity, the amplitudes of the z-component of angular momentum carried off by the electromagnetic radiation are the same as the substate amplitudes of the 2^+ excited state. Thus, the angular correlation of the gamma rays and inelastic protons reveals the substate populations, so long as the life time of the excited state is short enough so that it "remembers" the spin state in which it was created.

If we designate by $a_m \exp i\alpha_m$ the substate amplitudes, where $-2 \leq m \leq 2$, then it can be shown that the angular correlation function is given, for two specific cases, by the formulas

$$W(\theta_\gamma = 0, \phi_\gamma, \phi_p) = \frac{5}{8\pi} \left(a_1^2 + a_{-1}^2\right), \tag{1}$$

$$W(\theta_\gamma = \pi, \phi_\gamma, \phi_p) = \frac{5}{4\pi}\left[\left(\frac{a_1 - a_{-1}}{2}\right)^2 + \left(\frac{a_2 - a_{-2}}{2}\right)^2 + a_1 a_{-1} \sin^2(\phi_\gamma - \phi_1)\right.$$

$$\left. + a_2 a_{-2} \sin^2 2(\phi_\gamma - \phi_2)\right]. \tag{2}$$

The definitions for the angles in eqs. 1 and 2 are indicated in Fig. 7-1. The symmetry angles are related to the phases by the relations $2\phi_1 = \alpha_1 - \alpha_{-1}$, $4\phi_2 = \alpha_2 - \alpha_{-2}$. Also shown in Fig. 7-1 are the radiation patterns for pure (ℓ, m) radiation. The correlation functions, of course, contain coherent interference terms, but these are particularly simple for the two specific cases given by eqs. 1 and 2. It will be noted that eq. 1 is the "out-of-plane" perpendicular correlation, and eq. 2 the "in-plane" correlation.

Eq. 2 is often quoted in the literature in the form obtained by setting

$$\frac{4\pi}{5}A = \left(\frac{a_1 - a_{-1}}{2}\right)^2 + \left(\frac{a_2 - a_{-2}}{2}\right)^2, \tag{3}$$

$$\frac{4\pi}{5}B = a_1 a_{-1}, \tag{4}$$

$$\frac{4\pi}{5}C = a_2 a_{-2}. \tag{5}$$

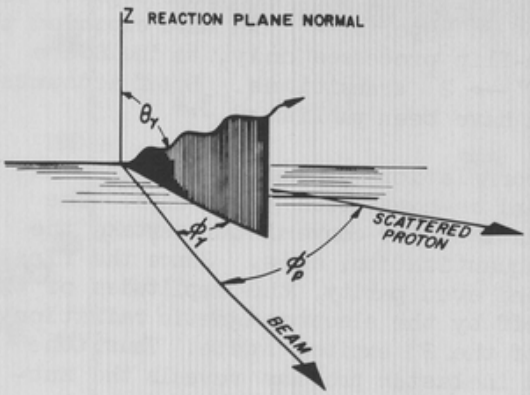

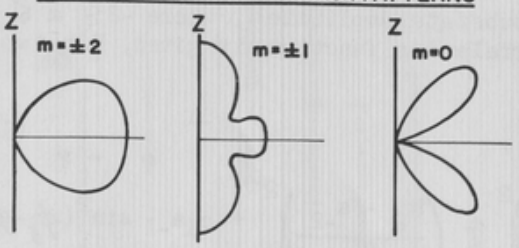

Figure 7-1

(a) Definition of angles for (p, γ) angular correlation.
(b) Radiation patterns for pure $\ell = 2$ multipoles. Each pattern is symmetric about the z-axis.

However, when one does this the clear physical significance of the terms is lost. We note that the isotropic term, A, is zero only if states of opposite J_z are equally populated. The presence of an isotropic term may thus indicate nuclear polarization of the excited state. The $\sin^2 \phi_\gamma$ term clearly arises from interference between +1 and -1 substates, and the $\sin^2 2\phi_\gamma$ term from interference between +2 and -2 substates. Plane wave approximations immediately predict $a_1 = a_{-1}$ and $a_2 = a_{-2}$, so that $A = 0$. Further, the symmetry axis, ϕ_2, lies along the direction of nuclear recoil.

The amplitudes are normalized, so that

$$\sum_i a_i^2 = 1. \tag{6}$$

If now we write for the a's in eq. 1

$$D = a_1^2 + a_{-1}^2 , \tag{7}$$

then the five equations 3, 4, 5, 6, and 7 can be solved for the magnitude of the substate amplitudes. The results are:

$$2a_{\pm 1}^2 = D \pm \sqrt{D^2 - 4B^2} , \tag{8}$$

$$2a_{\pm 2}^2 = D \pm \sqrt{E^2 - 4C^2} , \tag{9}$$

$$\text{where } E = 4A + 2B + 2C - D , \tag{10}$$

and a_o is given by eq. 6. The $\pm$ signs can be exchanged in any combination.

We note that ambiguities remain between states of opposite J_z. This is because the gamma radiation is symmetrical for + or $-J_z$. Only a circular polarization correlation measurement can determine the signs. Apart from these ambiguities it is clear that by means of two angular correlation measurements, one with the gamma ray detector in the plane of the reaction and the other with the gamma detector along the z axis, one can determine the values of the substate amplitudes. We refer to the two types of measurements as "in-plane" and "out-of-plane," respectively.

As pointed out in last year's report[2], a further physical interpretation can be given to the out-of-plane correlation (eq. 1); viz., that this correlation is not zero only if the inelastically scattered proton undergoes spin-flip in the scattering process. We therefore also refer to the out-of-plane correlation as the "spin-flip" measurement. The justification for this interpretation rests upon a theorem by A. Bohr[5] based on the fact that the reaction should, if parity and angular momentum are conserved, exhibit reflection symmetry through the plane of the reaction. This principle is sufficient to show that only if spin-flip occurs can the states with z component of angular momentum along the reaction plane normal equal to $\pm$ 1 be excited. One can also choose the nuclear recoil direction as the axis of quantization. However, the physical interpretation in terms of spin-flip is then lost.

It will be noted that the angular correlation function, $W(\theta_\gamma, \phi_\gamma, \phi_p)$, may depend upon the scattering angle ϕ_p. This dependence arises, of course, through the possible dependence of the amplitudes, $a_m \exp i\alpha_m$, on ϕ_p. It is, in fact, the ultimate objective of the experiment to map out the entire angular distribution of substate amplitudes. These, in turn, will be sensitive to the details of a particular nuclear model.

A simplified schematic diagram of the experimental arrangement used for the out-of-plane measurement is shown in Fig. 7-2. The detectors are mounted in the 60-inch scattering chamber. The angle of the proton detector may be altered remotely. Many complicating details, such as amplifiers and various monitoring scalers, have been omitted from the circuit diagram of Fig. 7-2. The arrangement for the in-plane measurements is similar. In this case the NaI (Tl) detector is situated in the plane of the reaction; it is physically supported on the rotating "table" of the scattering chamber so that its angle with respect to the beam may be adjusted.

As indicated in Fig. 7-2, the scheme of recording both the "gated" and "ungated" proton spectra enables us easily to correct the observed coincidence rate for accidentals. In addition, as will be shown later, the "ungated" proton counts are required for the data analysis. The accidentals arise from two scattering events occurring within the same cyclotron beam pulse. We have found that this procedure of continual measurement of the accidentals is absolutely essential, because the fraction of accidentals can vary widely from one measurement to the next. The variation is not due only to fluctuations in beam intensity; it is due to considerable changes in the beam duty cycle. These changes depend critically on the exact adjustment of the cyclotron and

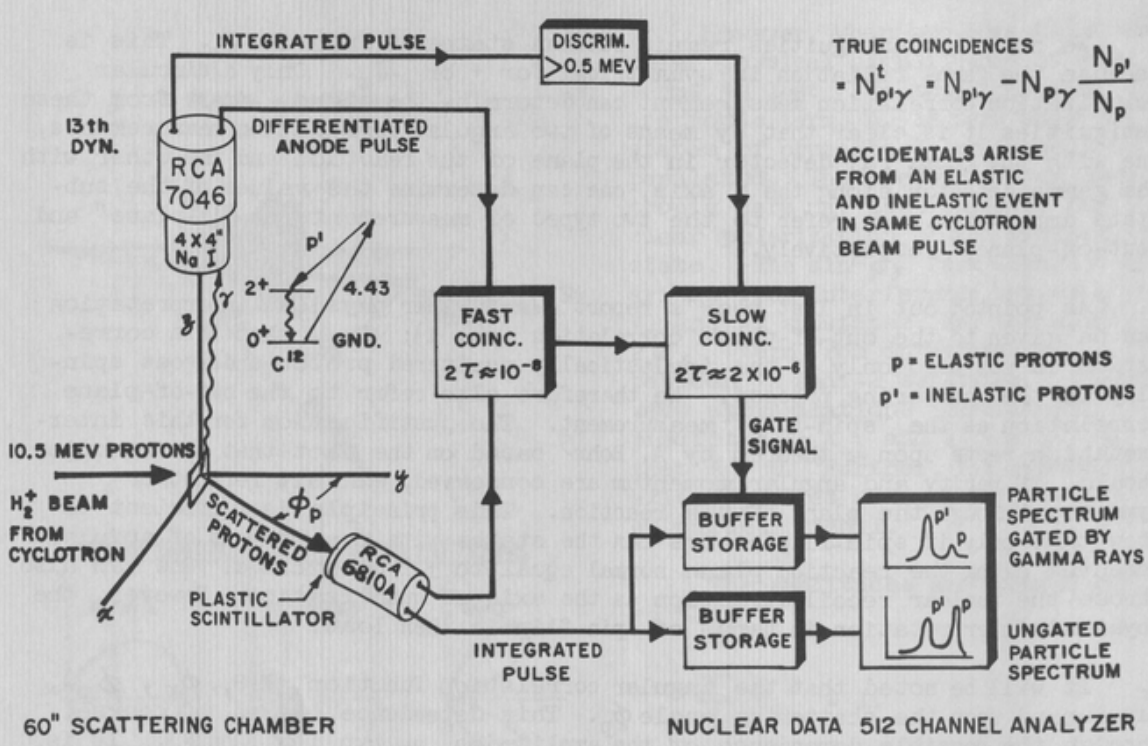

Figure 7-2

Schematic diagram of the experimental arrangement. Many details of the electronic set-up are omitted. Simultaneous display of the coincidence and raw spectra permits a continuous check of accidental coincidences.

external beam system. A further discussion of the problem of accidental counts is given in reference 6.

The angular correlation functions, eqs. 1 and 2, imply that to utilize this method for determining the amplitudes a_m requires an absolute measurement of the coincidence rates. We designate by ϵ_γ the total efficiency of the gamma counter, and by F that fraction of the total gamma ray spectrum lying above the discriminator level, as shown in Fig. 7-2. The true coincidence rate is then given by

$$N^t_{p'\gamma} = F\,\epsilon_\gamma\,N_{p'}\int W(\theta_\gamma, \varphi_\gamma, \phi_p)\,d\Omega_\gamma \qquad (11)$$

where the integral extends over the solid angle subtended by the gamma counter. $N_{p'}$ is the counting rate in the inelastic peak of the proton spectrum corresponding to excitation of the (single) gamma transition.

In general, $W(\theta_\gamma, \phi_\gamma, \phi_p)$ will contain complicated interference terms, so that its form will be difficult to handle. However, for circular symmetry about the z axis, the interference terms all cancel out, so that the integral in eq. 11 may be written as the sum of pure (ℓ, m) multipole distribution functions (Fig. 7-1) multiplied by the amplitudes a_m:

$$\int_{z\ axis} W(\theta_\gamma, \phi_\gamma, \phi_p)\, d\Omega_\gamma = \int \left[a_o^2 W_o + (a_1^2 + a_{-1}^2) W_1 + (a_2^2 + a_{-2}^2) W_2 \right] d\Omega_\gamma . \quad (12)$$

where the W's are the gamma distribution functions for pure $(\ell = 2, \pm m)$ radiation. If the solid angle subtended by the gamma detector is small, then, as indicated by the diagrams in Fig. 7-1, W_o and W_2 are small and may be neglected. Eqs. 11 and 12 can be solved to give the probability for spin-flip.

$$D = a_1^2 + a_{-1}^2 = \frac{N^t_{p'\gamma}}{F\, \epsilon_\gamma\, N_{p'}\, W_1\ (\theta_\gamma = 0)\ \Delta\Omega_\gamma} . \quad (13)$$

For the case where we are not justified in neglecting the radiation due to $m = \pm 2$ and $m = 0$, we obtain

$$a_1^2 + a_{-1}^2 = \frac{N^t_{p'\gamma}}{F\, \epsilon_\gamma\, N_{p'}} \frac{\int \left[W_2 + a_o^2 (W_o - W_2) \right] d\Omega_\gamma}{\int (W_1 - W_2)\, d\Omega_\gamma} \quad (14)$$

The amplitudes $a_{\pm 2}$ do not appear in eq. 14 because of the normalization condition, eq. 6.

Eq. 14 shows that we must know a_o^2 in order to find $a_1^2 + a_{-1}^2 = D$. In practice, we neglect the effect of a_o^2 on the spin-flip, calculate a_o^2 by means of the eqs. 7 to 10, then insert this value of a_o^2 into eq. 14 to obtain the corrected spin-flip. Actually, the effect of a_o^2 for the geometry of our gamma detector is small. It amounts to a correction of only 7 per cent to the spin-flip, even for the extreme case of $a_{\pm 2} = 0$.

Several comments should be made concerning the quantities $\Delta\Omega_\gamma$, ϵ_γ, and F which appear in eqs. 13 and 14. A knowledge of $\Delta\Omega_\gamma$ implies that the beam spot on the target is small compared with the dimensions of the lead collimator of the gamma detector. This is not the case, so we have devised a measurement utilizing a "standard" point target, the counting rates from which can be compared with the actual finite sized target. The details of the technique will not be discussed, but it enables us to make a continuously

measurable correction to the solid angle factor which takes into account fluctuations such as the beam position on the target. The scheme works also for the "in-plane" correlation measurement.

The value for ϵ_γ, the total efficiency of the gamma detector, is taken from standard tables. However, there may well be an error in this number due to geometrical effects. In the near future we plan to make a direct measurement of ϵ_γ. As for F, the fraction of the total gamma spectrum accepted by the electronic system, we measure this quantity by displaying the gamma spectrum on a multichannel analyzer and observing the fraction above the discriminator level. For the spin-flip measurement, any shifts in the discriminator level or in gain are automatically corrected for by means of the "standard" target calibration. However, for the in-plane correlation it is necessary continuously to monitor the gamma ray spectrum. Our procedures for accomplishing this are not yet perfected, and the results we have obtained to date are to be regarded as tentative.

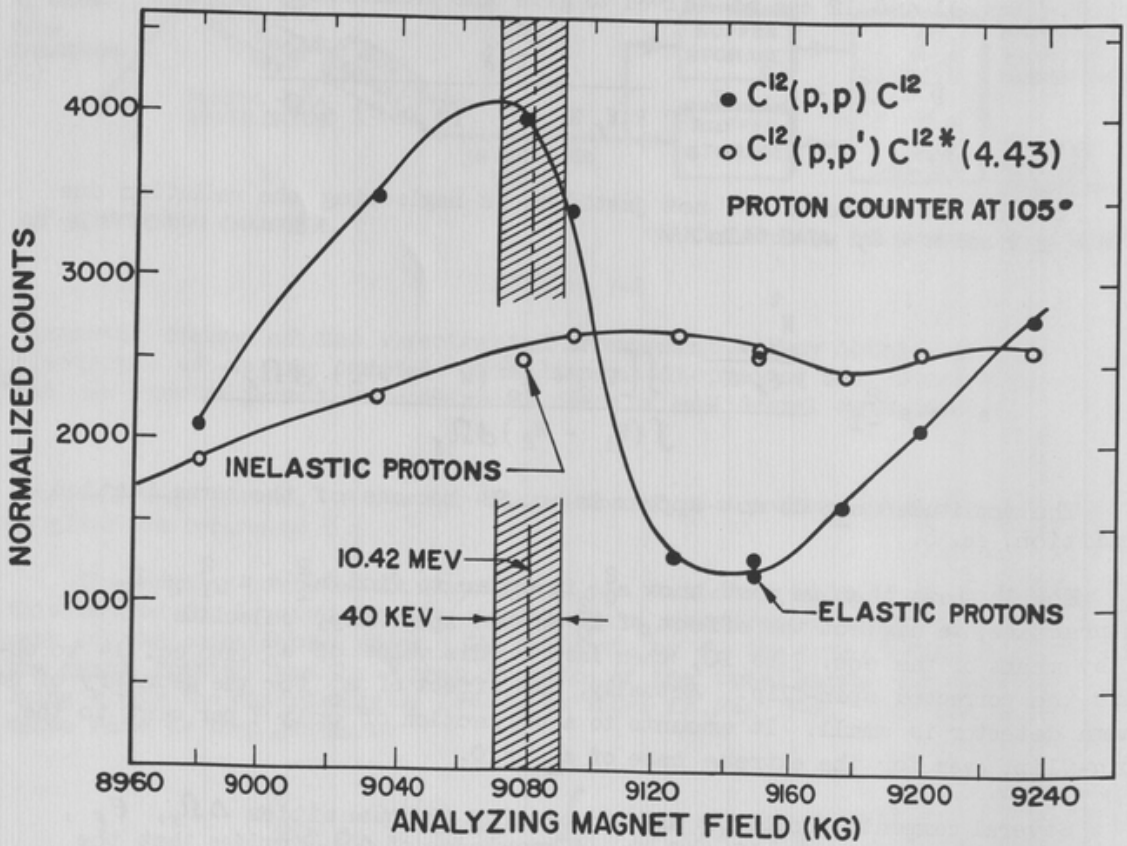

Figure 7-3

Elastic and inelastic cross sections for protons on C^{12} at 105° vs. beam analyzer field. The shaded portion corresponds to the energy range used in the (p, γ) correlation measurements. It is centered at 10.42 Mev and has a width of 40 Kev.

Our investigations thus far have been confined to the C^{12} (p, p'γ)C^{12} (4.43 Mev) reaction. We chose this reaction firstly because of ease in obtaining suitable target material and secondly because it has a particularly simple spectrum. After we were well under way we found that a level in N^{13} occurs at very nearly 10.5 Mev bombarding energy. In Fig. 7-3 we show our measurements of the elastic and inelastic cross sections at 105° vs. energy. The cyclotron energy was varied by moving the ion source in and out. The resonance has recently been investigated by several groups.[7,8] Our spin-flip and in-plane correlation measurements have been confined to the energy band indicated on Fig. 7-3.

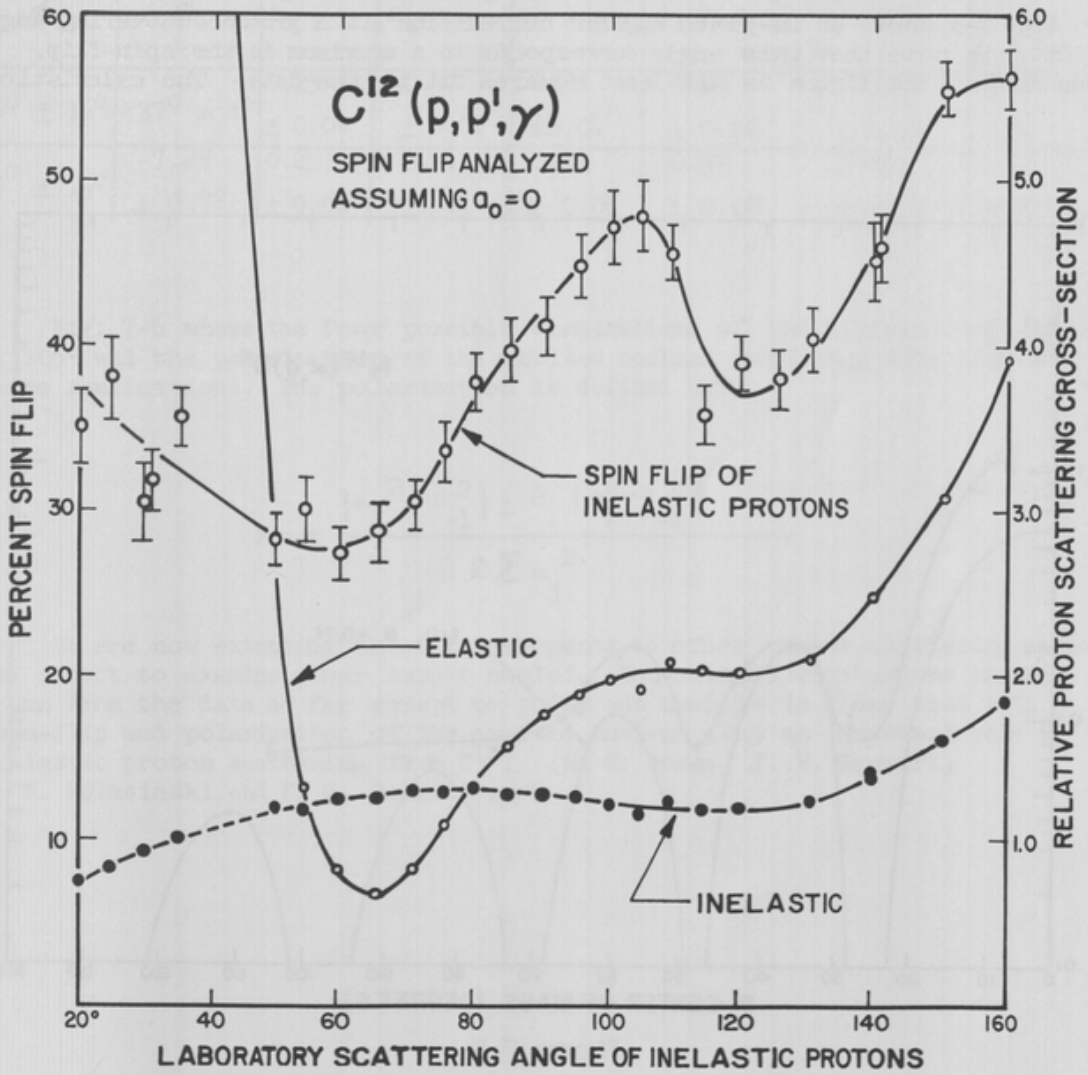

Figure 7-4

Spin-flip vs. scattering angle for C^{12} (p,p')C^{12}. For comparative purposes, the elastic and inelastic cross sections are also shown.

Fig. 7-4 shows our results of the spin-flip measurement vs. proton scattering angle. Shown also, for comparison, are the elastic and inelastic angular distributions. The per cent spin-flip is the quantity D defined by eq. 7. a_o^2 is assumed to be zero for Fig. 7-4; if all other inelastic scattering is due to the a_o term, the spin-flip is about 7% less than shown.

The most notable feature of Fig. 7-4 is that the spin-flip is far from constant; moreover, it exhibits more structure than the inelastic angular distribution.

Fig. 7-5 shows an in-plane angular correlation at a proton scattering angle of 105°. We note that this angle corresponds to a maximum in the spin-flip. Shown also on the figure is the least squares fit to the data. The calculation

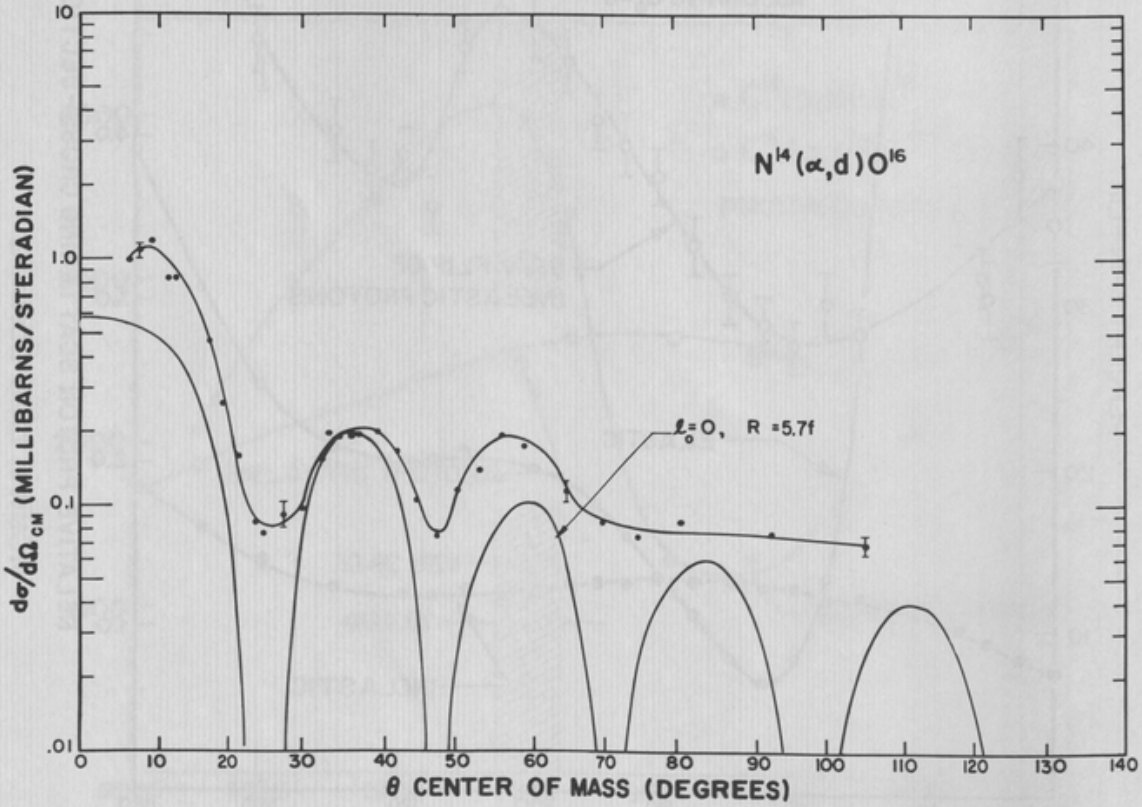

Figure 7-5

In-plane angular correlation. The solid curve was fitted to the data with the aid of an IBM 709 computer.

was carried out on the IBM 709 computer at the University of Washington Computer Center. The results for two complete measurements are given in Table 7-1. The scattering angle of 60° corresponds to a minimum in the spin-flip.

Table 7-1.

ϕ_p	ϕ_1	ϕ_2	a_0^2	$a_1^2 + a_{-1}^2$	$a_2^2 + a_{-2}^2$	$\frac{\lvert a_1^2 - a_{-1}^2 \rvert}{a_1^2 + a_{-1}^2}$	$\frac{\lvert a_2^2 - a_{-2}^2 \rvert}{a_2^2 + a_{-2}^2}$	% Polarization
105°	16° ± 16°	37° ± 1°	0.25	0.44	0.31	0.98	0.85	± 48
			± 0.04	± 0.02	±0.04	± 0.06	± 0.18	± 5
60°	75° ± 19°	-7.2°	0.25	0.241	0.51	0.99	0.69	± 47
		± 0.7°	± 0.06	±.014	± 0.06	± 0.08	± 0.19	± 23

Fig. 7-6 shows the four possible combinations of the substate amplitudes at 105° and the polarization of the excited nucleus resulting from each of these combinations. The polarization is defined by:

$$P = \pm \frac{\lvert a_1^2 - a_{-1}^2 \rvert \pm 2 \lvert a_2^2 - a_{-2}^2 \rvert}{2 \sum a_j^2}$$

We are now extending these measurements to other proton scattering angles and expect to examine other target nuclei. No detailed conclusions can be drawn from the data so far except to point out that it is clear that both spin-flip and polarization of the excited nucleus play an important role in inelastic proton scattering from C^{12}. (R. E. Brown, J. B. Gerhart, W. A. Kolasinski, and F. H. Schmidt).

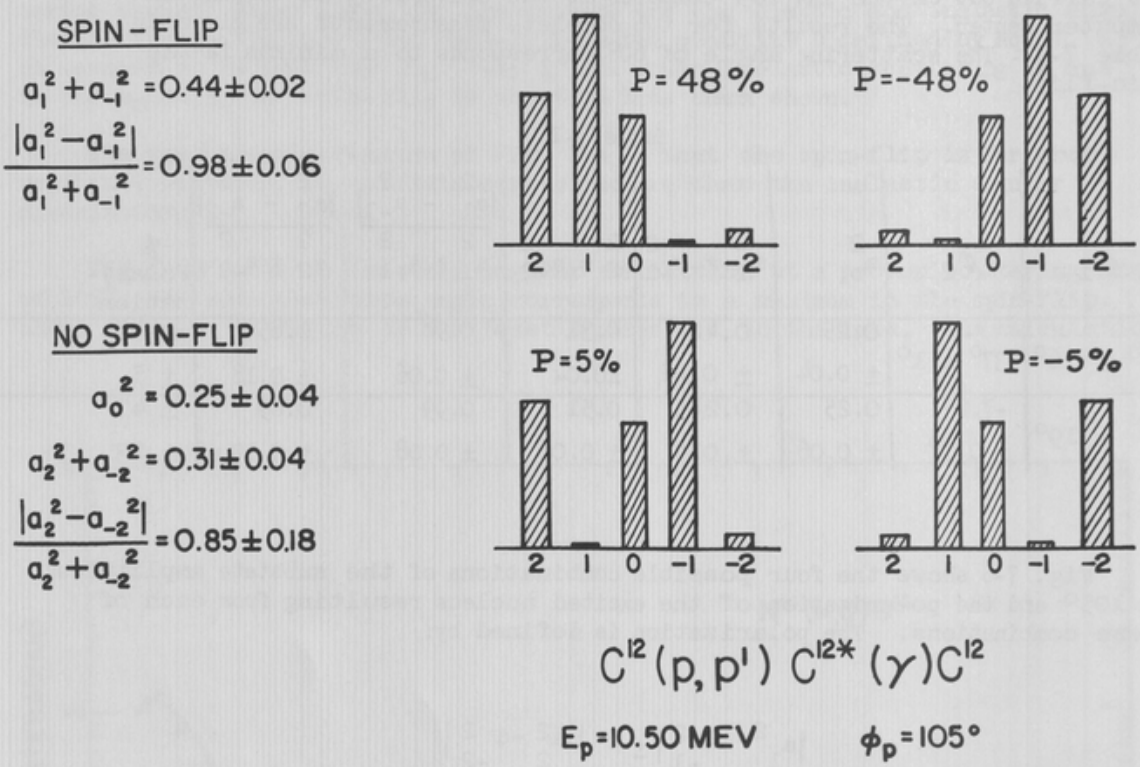

Figure 7-6

Histograms illustrating the four possible substate populations compatible with the experimental data. The corresponding nuclear polarization is indicated for each case. A choice between the four possibilities cannot be made without circular polarization correlation measurements.

1 Cyclotron Research, University of Washington (1960), p. 23.
2 Cyclotron Research, University of Washington (1961), p. 37.
3 F. H. Schmidt, J. B. Gerhart, and W. A. Kolasinski, Bull. Am. Phys. Soc. 7, 60 (1962).
4 J. B. Gerhart, F. H. Schmidt, W. A. Kolasinski, and R. E. Brown, Bull. Am. Phys. Soc. 7, 270 (1962).
5 A. Bohr, Nuclear Phys. 10, 486 (1959).
6 Cyclotron Research, University of Washington (1961), p. 44; F. H. Schmidt, J. Orth, and H. Fauska, Proceedings of Belgrade Conference on Nuclear Electronics (I.A.E.A.) (to be published).
7 V. R. McKenna and G. G. Shute, Australian J. of Phys. 14, 432 (1961); V. R. McKenna, A. M. Baxter, and G. G. Shute, Australian J. of Phys. 14, 196 (1961).
8 H. S. Adams, J. D Fox, N. P Heydenburg, and C. M. Temmer, Phys. Rev. 124, 1899 (1961).

III. NUCLEAR FISSION

8. Ternary Fission at Moderate Excitation Energies

Sometimes the spontaneous fission of the transuranium elements occurs with division into two heavy fragments and one light fragment of long range, usually an alpha particle[1,2]. The ratio of these ternary fission events to normal binary events is 1:300 to 1:400. These third particles are thought to be produced at the moment of scission and it is hoped that studies of their distributions may reveal information concerning the scission process as distinct from saddle point phenomena.

During the past year, nuclear counter investigations of the distributions of long-range particles from ternary fission at moderate excitation energies have continued. Solid state radiation detectors and a fast-slow coincidence circuit have been used to observe the coincident fragments from helium ion and proton induced ternary fission of U^{238} and Th^{232}. The detection system was calibrated with a spontaneous fission source Cf^{252}.

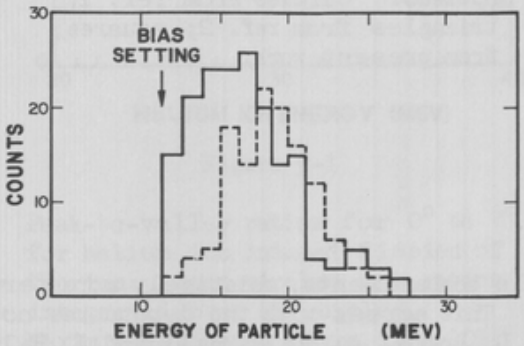

Figure 8-1

Spectrum of long-range particles in coincidence with heavy fragments in the fission of Th^{232} with 42.5 Mev helium ions (including 13% accidental counts). The dashed curve shows a similar spectrum observed in the spontaneous fission of Cf^{252}.

The relative probability of ternary to binary fission induced in Th^{232} and U^{238} with 42 Mev helium ions is approximately the same as that observed in spontaneous fission of elements in the same region as the compound nuclei formed in the helium ion bombardments. Figures 8-1 and 8-2 show some preliminary results from the bombardment of Th^{232} with helium ions. These observations were made at 135° with respect to the direction of the helium ion beam. Large solid angles were used.

In 10.5 Mev proton induced fission of Th^{232} and U^{238} the relative ternary fission probability is less by a factor of 2 to 3 than it is for spontaneous or slow neutron fission. (See Fig. 8-3). This decrease with increasing excitation energies continues the trend from spontaneous to slow neutron fission observed by Nobles and Mostovoi[3]. It suggests that the higher yields observed in the bombardment with 42 Mev α particles may be due to factors other than excitation energy; for example, the effects of angular momentum on the rate of the tearing process at scission.

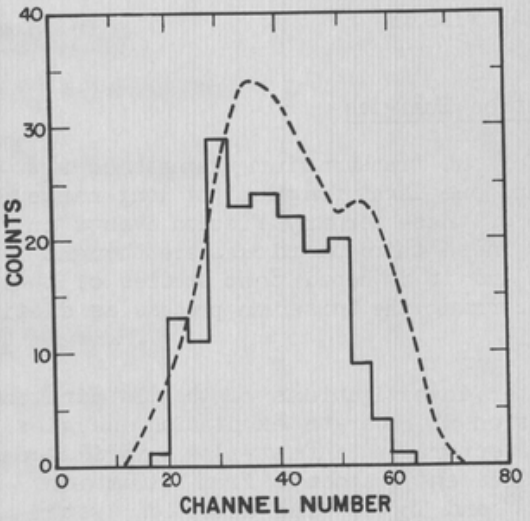

Figure 8-2

Spectrum of heavy fragments in coincidence with long-range particles in the fission of Th^{232} with 42.5 Mev helium ions (including 13% accidental counts). The dashed curve shows the spectrum of fission fragments not in coincidence with long-range particles.

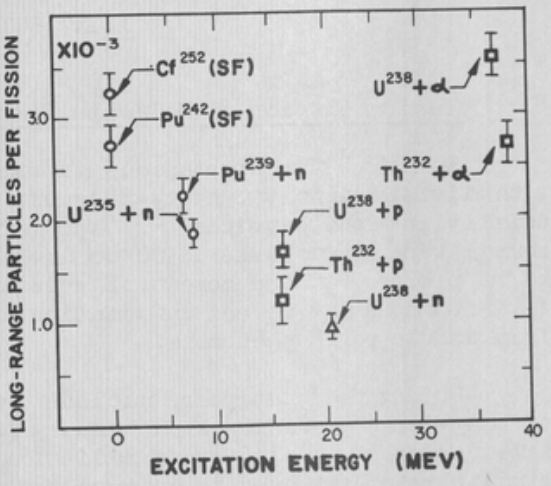

Figure 8-3

The number of long-range particles per fission vs. the excitation energy of the initial compound nucleus. Circles from ref. 1; triangles from ref. 2; squares from present work.

For both the proton and alpha particle bombardments, relatively more ternary events are observed from U^{238} than Th^{232}. This agrees with the dependence noted in spontaneous fission[1]. (J. A. Coleman, D. Drake, A. W. Fairhall and I. Halpern.)

---

1 R. A. Nobles, "Long-Range Particles from Nuclear Fission," Thesis, University of New Mexico, 1961.
2 H. E. Wegner, Bull. Amer. Phys. Soc. 6, 307 (1961).
3 V. I. Mostovoi, Proc. Intern. Conf. Peaceful Uses Atomic Energy, Geneva (United Nations, New York, 1955), Vol. 2, p. 226.

---

9. Ba^{139} / Ag^{113} Ratios in the Fission of Uranium

A radiochemical study of the relative "peak" and "valley" mass yields as a function of angle for the Th (α, xnf) reactions has been completed. Observations of Ba^{139} / Ag^{113} ratios were made at small forward angles by radiochemical separation of fission fragment recoils. Ratios integrated over all angles were obtained by radiochemical separation in a stacked foil. A sample of the results is shown in Fig. 9-1. The compound nucleus formed in the bombardment, U^{236}, may decay by fission or by neutron emission. A similar competition occurs at each stage along the neutron evaporation chain. The yield ratio Ba^{139} / Ag^{113} at each stage is presumably characteristic of the fissioning species and its excitation energy. The increase in the yield of Ba^{139} relative to Ag^{113}, due to the onset of the (α, 3nf) reaction at 24 Mev, is clearly evident in Fig. 9-1. The expected rise at 32 Mev because of the onset of the (α, 4nf) reaction is not observed. The suppression of the relative yield of Ba^{139} indicates that relatively few nuclei survive to fission at low excitation energies. One factor which could affect this survival is the angular momentum of the system. Fissionability increases with angular momentum of the fissioning species.[1] The angular momentum imparted to a compound nuclei (U^{236}) by incident helium ions with energies (30 Mev) above the Coulomb barrier (24 Mev) is large compared to that by particles with energies near the barrier. Thus, the relatively large amount of angular momentum in the compound system at the onset of the (α, 4nf) reaction may cause fission to occur earlier in the evaporation chain.

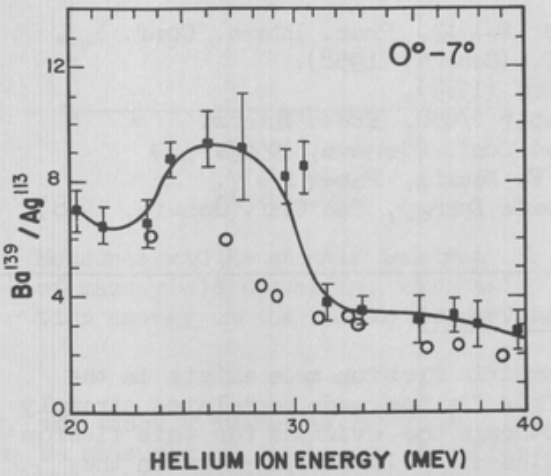

Figure 9-1

Peak-to-valley ratios for 0° to 7° for helium ion induced fission of thorium. Open circles are ratios integrated over all angles. Maximum estimated error is ± 10%.

A reconstruction of the experimental observations has been attempted, using empirical data and present ideas of the fission process. These calculations include the following parameters: angular distributions[2], evaporated neutron energy spectra, fissionability[3,4], and mass yields[5]. Although qualitative agreement with the experimental results is obtained, quantitative agreement is poor. This leads one to reconsider some of our present ideas of fission; in particular, fissionability and mass yields at various stages along a neutron evaporation chain. A crude calculation shows that Γ_f/Γ_n

values can be increased by factors of 1.2 to 3 at low excitation energies (later stages in the neutron emission chain) if one considers the possible amounts of energy tied up in rotation. Also, the yields of asymmetric fragments in the symmetric fission mode which is assumed to predominate at excitation energies above 20 Mev, may be larger than we think[6]. Computer calculations are now being used to facilitate the study of the angular momentum dependence of fissionability and the energy dependence of mass yields in an attempt to achieve quantitative agreement with observed peak-to-valley ratios. (J. A. Coleman and A. W. Fairhall.)

---

1 J. Gilmore, "The Effect of Angular Momentum on Fission Probability," Thesis, UCRL-9304, (1960).
2 I. Halpern and V. M. Strutinski, Paper P/1513, Proc. Intern. Conf. Peaceful Uses Atomic Energy, 2nd Conf. (Geneva, 1958).
3 I. Halpern, Ann. Rev. Nucl. Sci. 9, 267 (1959).
4 R. Vandenbosch and J. R. Huizenga, Paper P/688, Proc. Intern. Conf. Peaceful Uses Atomic Energy, 2nd Conf. (Geneva, 1958).
5 A. W. Fairhall, R. C. Jensen, and E. F. Neuzil, Paper P/677. Proc. Intern. Conf. Peaceful Uses Atomic Energy, 2nd Conf.(Geneva, 1958).
6 See Sec. 10 of this report.

---

10. Fission Studies in Bismuth and Lead Targets

It has been reported[1] that an asymmetric fission mode exists in the fission of Bi^{209} with 36 Mev protons. This fission mode correlates strongly with magic numbers N = 82 and Z = 50, although the evidence for this fission mode comes from observations on the complementary light fragments in the region of zinc. It would seem to be desirable to obtain further information on this interesting development. The same compound nucleus excited to a comparable excitation energy can be made by bombarding Pb^{206} with 42 Mev He ions. These experiments have been carried out, but the results are inconclusive owing to the presence of Fe, Ni, Zn, and Cu impurities in the Pb^{206} target. Attempts to purify the target material by ion exchange and zone refining are under way. The refined material will be reinvestigated in an effort to confirm the existence of asymmetric fission in this element region.

Mass-yield curves for fission of lighter elements (Au, Pb, Bi targets) are all single humped, corresponding to symmetric fission[2,3]. A separate symmetric fission mode is also observed in radium bombarded by neutrons[4], protons[5], deuterons[6], and gamma rays[7]. Within the experimental errors these mass-yield curves are Gaussian in shape. An interesting feature is that they vary in width, usually expressed as width at half-maximum. In Figure 10-1, the observed widths at half-maximum ($W_{1/2}$) are plotted vs. excitation energy at the saddle point (E^*_{SP}). The latter is obtained by subtracting the fission threshold energy[8] from the excitation energy of the compound nucleus (symmetric fission is essentially all first-chance fission). It is seen that the widths of the mass-yield curve appear to increase linearly with excitation energy over this limited energy interval. It should be emphasized that a wide range of experimental conditions prevails: target elements range from gold to radium;

bombarding energies range from 11 to 42 Mev; and bombarding particles include neutrons, protons, deuterons, He^3 and He^4.

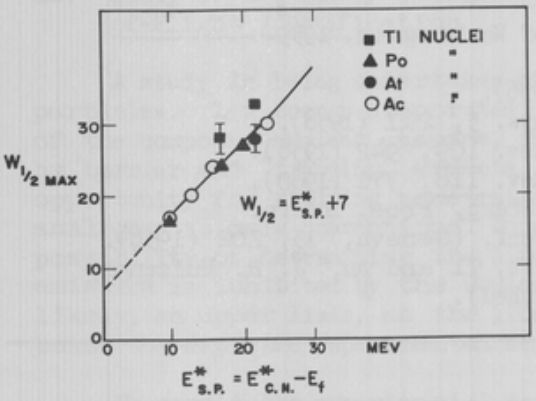

Figure 10-1

Measured widths at half maximum of mass-yield curves vs. excitation energy at the saddle point.

From simple statistical theory one might expect the relative yields of two fission products to be of the form

$$\frac{Y_1}{Y_2} \sim e^{-c\,(E_1 - E_2)\ /T}, \qquad (1)$$

where E_1 and E_2 are the energies required to form the products and T is the nuclear temperature. On the other hand, a Gaussian yield curve implies the yields are of the form

$$\frac{Y_1}{Y_2} \sim e^{-(A_1 - A_2)^2\ /\ W^2_{1/2}} \qquad (2)$$

where A_1 and A_2 are the respective mass numbers. Comparison of equations (1) and (2) implies that W^2 varies with T, and since T varies as $E^{1/2}$, $W_{1/2}$ should be proportional to $E^{1/4}$. Here E is to be measured at the point where the mass distribution is determined. Presumably this point is the moment of scission where the corresponding energy is perhaps of the order of 10 Mev higher than the excitation energy at the saddle point.

The data of Fig. 10-1 can be replotted vs. $E^{1/4}$ and will be found to cluster on a straight line. However, the straight line does not pass through the origin as equations (1) and (2) would imply. Thus this simple picture is not correct and a more refined theory is necessary to explain the apparent correlation.

Perhaps the correlation shown in Fig. 10-1 is accidental. Further experiments are in progress with Pb, Bi and Au targets to obtain more data in an effort to establish the validity of the correlation. It is also hoped that it will be possible to better characterize the true dependence of $W_{1/2}$ on excitation energy. (A. W. Fairhall and R. L. Watters.)

1 T. T. Sugihara, J. Roesmer and J. W. Meadows, Jr., Phys. Rev. 121, 1179 (1961).
2 E. F. Neuzil, Ph.D. Thesis, University of Washington, 1959 (unpublished).
3 A. W. Fairhall, Phys. Rev. 102, 1335 (1956).
4 R. A. Nobles and R. B. Leachman, Nuc. Phys. 5, 211 (1958).
5 R. C. Jensen and A. W. Fairhall, Phys. Rev. 109, 942 (1958).
6 R. C. Jensen and A. W. Fairhall, Phys. Rev. 118, 771 (1960).
7 R. B. Duffield, R. A. Schmitt and R. A. Sharp, Proc. Intern. Conf. Peaceful Uses Atomic Energy, 2nd Conf. (Geneva,) 15, 202 (1958).
8 Eq. 8 of "He-ion Induced Fission of Bi, Pb, Tl and Au," J. R. Huizenga, R. Chaudhry, and R. Vandenbosch (unpublished).

IV. COMPOUND NUCLEAR REACTIONS

11. Study of Low Energy Charged Particle Evaporation Using Time-of-Flight Identification

A study is being undertaken of the evaporation of low energy charged particles. Low energy evaporated particles are emitted primarily at the end of the compound nuclear cascade, and their spectra are strongly influenced by barrier and "trapping" effects. The study of the spectra affords an opportunity for studying penetration of the nuclear surface. Through a method analogous to more conventional Doppler shift methods, it may also offer the possibility of determining the lifetime for "trapped" charged particles whose emission is inhibited by the Coulomb and angular momentum barriers (or more likely, an upper limit, as the lifetime for competing gamma rays is probably below the expected experimental sensitivity of about 10^{-13} to 10^{-14} seconds).

To permit the experimental examination of low energy charged particles, a system is being developed for particle identification and energy determination based on the independent measurement of energy and time-of-flight. The system uses a solid-state particle detector to provide a "slow" pulse, which gives energy information in the usual way, as well as a "fast" signal. By the techniques developed for fast neutron spectroscopy at this laboratory[1], the fast signal gives time-of-flight information when compared to a cyclotron oscillator timing signal in a time-to-pulse-height converter.

The energy (E) and flight time (T) pulses are amplified and stretched, and are then displayed as a single spot with coordinates (T, E) on the horizontal and vertical deflection axes of an "x-y" oscilloscope. The spots form a family of curves; each curve corresponds to a different mass of reaction product.

For the convenient choice of flight path of 0.65 m, which is somewhat less than the radius of the 60-inch scattering chamber, a proton energy range of 10 Mev to 1 Mev corresponds to flight times between 15 and 50 nanoseconds. For heavier particles, the energy limits for the same flight time interval are increased by the appropriate mass ratio. The maximum convenient flight time is determined by the cyclotron duty cycle of 87 nanoseconds, and the minimum time by the overall resolution of the time-of-flight circuitry.

One difficulty with using the "fast" pulse furnished by the solid-state detector was that its magnitude (about 1 millivolt) was comparable to possible sources of noise or pickup, especially the 11.7 Mc radio-frequency signal from the cyclotron oscillator. This difficulty was solved by placing the detector inside a shielding box, which also contains a transistorized fast amplifier and a wavetrap tuned to the cyclotron frequency.

A systematic, energy-dependent distortion of the time-of-flight measurement occurs because of the time required for the fast pulse to rise to the triggering threshold of the timing circuitry. The maximum energy of reliable particle identification is determined by this distortion, by the penetration

of a "thin" detector at high incident particle energies, and by the time resolution of the electronic system.

The present, preliminary, system, using one particular diffused-junction type solid state particle detector capable of stopping about 5 Mev protons, has an overall energy resolution of 250 kev and time resolution of approximately 7 nanoseconds. The system distinguishes between protons in the energy range from 0.8 to 3 Mev, deuterons from 1.5 to 5 Mev, and alpha particles from about 2 to 20 Mev. It does not clearly distinguish between mass three and mass four particles. It is expected that a wider energy range and better mass and energy resolution will be obtained by the use of a surface barrier detector of greater sensitive depth and better energy resolution. (D. Bodansky and E. R. Parkinson.)

---

1 Cyclotron Research, University of Washington (1961), p. 34.

---

12. Angular Distributions of Neutrons in Bombardments with 42-Mev Alpha Particles [1]

The time-of-flight neutron spectrometer described in previous reports was completed and tested during the past year, and it has been used for a series of measurements with 42-Mev alpha particles.

The spectrometer system now has the following features:

(1) The neutron detector is a stilbene crystal (3.81 cm dia. x 2 cm thick) viewed by a 6810A photomultiplier. It is located 173 cm from the center of the 60-inch scattering chamber. This puts the center of the crystal about three feet outside the chamber.

(2) Because of the large photon and neutron backgrounds in the scattering room, it is necessary to surround the crystal with a large shield of lead, wax, and borax. The shield and counter are mounted on wheels and can be moved from angle to angle around the scattering chamber.

(3) Backgrounds are measured by plugging the collimator hole in the shield with an iron absorber long enough to attenuate the neutrons moving from the target to the crystal by a factor of 100. In a typical set of measurements, background runs of this type are occasionally supplemented with target-out background runs.

(4) The beam is monitored by scintillation detectors sensitive to scattered alpha particles and by the Faraday cup current. To obtain reliable current readings, it has been necessary to replace the old Faraday cup with a new one having a wider throat. The new cup permits the use of targets thicker than those normally used in experiments where emitted charged particles are detected.

(5) The efficiency of the detection system for neutrons is computed from the known neutron cross sections, the size of the crystal, and from data taken in runs to determine the pulse-height bias in the detection circuits. This bias is set by a discriminator which gates the multi-channel analyzer where the time-distribution is recorded.

(6) The analyzer can also be gated by a circuit which discriminates severely against pulses due to photons. This neutron-photon discriminator has proved very useful in the testing of the system, but it is not used when actual data are taken.

(7) A new time-to-pulse height converter has been built. It is flat in efficiency with respect to time to within 4 per cent in the interval normally used for neutron spectra. The time resolution is from 3 to 4 nanoseconds as determined from the width of the prompt photon peak.

(8) The energy vs. channel calibration is computed from the time calibration of the channels (obtained from the spacing between prompt photon peaks) and is checked by using absorbers like oxygen which have strong absorption lines for neutrons of certain energies.

(9) Two out of every three beam bursts from the cyclotron are eliminated by an rf flapper system which has been described in earlier reports.[1]

The first study undertaken with this system is that of the angular and energy distributions of neutrons emitted from Al, Co, Nb and Au in bombardments with 42-Mev alpha particles. Data were taken at 45°, 75°, 105°, 135°, and 165° in the laboratory. It was not possible to obtain reliable data forward of 45° because of background uncertainties.

One general object of these neutron studies is to compare them to corresponding studies of proton emission (see Sec. 13). It has been pointed out in previous reports[2] that the comparison of neutron and proton evaporation angular distributions might help determine which regions on the nuclear surface, with respect to the rotation axis, are responsible for most of the particle evaporation.

Preliminary results for the spectra and angular distributions of neutrons from the four targets studied are given in Fig. 12-1. The results are plotted as a function of angle in the center-of-mass system and they are labeled by neutron energy in Mev, also in the c.m. system. The curves are fits to the backward hemisphere data by the functional form $(1 + a \cos^2\theta)$. At low neutron energy there seems to be 90° symmetry and the forward data fit the same form. At higher energy they exceed it, presumably due to direct interactions, as indicated by the increasing gap between a smooth curve through the data and a symmetric curve (shown dashed) which fits the backward data. The data are new and are in the process of being analyzed. Some of the more significant features seem to be:

(1) The appearance of a direct interaction component (i.e. forward excess) at energies as low as 3.5 Mev (in Au). The direct interactions are

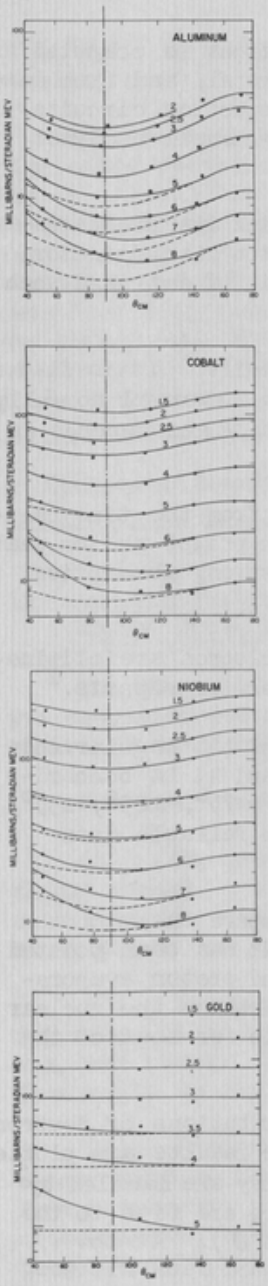

Figure 12-1

Angular distribution of neutrons from alpha particle bombardment of (a) aluminum, (b) cobalt, (c) niobium, and (d) gold.

evident as far back in angle as 90° at 5 Mev. The presence of this direct interaction would tend to confirm the conclusion of Sidorov[3] that some neutrons are emitted before thermal equilibrium is established.

(2) The anisotropy decreases as the target gets heavier. This is expected because the angular velocity induced in the heavier nuclei by 42-Mev alpha particles is smaller.

(3) The anisotropy of evaporated neutrons seems to stay fairly independent of neutron energy (although this point is somewhat obscured by the direct interaction component). This is a little unexpected because the elementary theory suggests that the anisotropy should go as E_n multiplied by a function varying only slowly with neutron energy. (For example, E_n = 0 neutrons must be isotropic, since they would have to be S-wave neutrons). Evaporation protons have been studied[4] in heavy ion bombardments and the anisotropy increases slightly with increasing proton energy. The maintenance of a large anisotropy at low neutron energy might be an indication that: (a) the low energy part of of the spectrum is strongly populated by neutrons evaporated from nuclei with the largest angular momentum. This would come about because these nuclei, having a considerable amount of energy tied up in rotation, would tend to emit low energy neutrons; (b) the moment of inertia becomes abnormally small at low excitation energies.

(4) The observed cross sections, the magnitudes of the anisotropies, and nuclear temperatures estimated from the data are in reasonable accord with expectations.

(5) In the course of the investigation, it was very easy to count the photons in the prompt photon peaks at each angle and the angular distributions were found to resemble those for neutrons, in that they were anisotropic with minima at 90°. The anisotropy decreased as the target mass increased. This photon anistropy is presumably due to the release of angular momentum through photon emission at the end of the particle-evaporation cascades. Further studies will be made of the emitted photons. (P. Axel, D. Drake, I. Halpern, R. Parkinson).

1 Cyclotron Research, University of Washington (1961), p. 34; (1960), p. 47.
2 Cyclotron Research, University of Washington (1961), p. 30.
3 V. A. Sidorov, Evaporation Spectra of Neutrons (Lenin Prize Institute of the Academy of Sciences of the USSR, Moscow, 1961).
4 W. J. Knox, A. R. Quinton, and C. E. Anderson, Phys. Rev. 120, 2120 (1960).

13. Spectra and Angular Distributions of Protons Emitted in Alpha Particle Bombardments

Investigations of proton evaporation processes described in last year's progress report have been continued. In this phase of the investigation, measurements are being made of proton energy and angular distributions, using a single proton detector. The problems under study include:

(1) Comparison of isotopes of the same element. Proton spectra from enriched targets of Ni^{58}, Ni^{60}, and Ni^{62} have been studied with the help of the dE/dx - E particle identification system described earlier[1]. The system very satisfactorily separates protons and deuterons from alpha particles when used with a 2 mil plastic dE/dx scintillator, but it does not separate protons from deuterons. It was found that proton-deuteron separation becomes possible when the thickness of the dE/dx scintillator is increased to 10 mils, but this raises the proton energy threshold of the detector from 2.5 to 4.5 Mev. Therefore, the present system produces proton spectra which are free from deuterons only above approximately 5 Mev. However, since the total deuteron yield is typically less than 10% of the total proton yield, and spectra taken with the 10 mil dE/dx crystal show the deuteron yield to be decreasing at 5 Mev while the proton yield is peaking, this contamination is not serious. For Ni^{58} (the most copious proton emitter studied) less than 2% of the observed spectrum below 5 Mev can be attributed to deuterons.

Fig. 13-1 shows proton spectra from Ni^{62} bombarded with 42-Mev alpha particles. These data are a combination of both the 2 and 10 mil results. This type of plot (i.e., angular distributions of the cross section taken at integer center-of-mass energies) was drawn because it displays the gross interdependences of yield, energy, and center-of-mass angle. The conversion of the data to the center-of-mass coordinates was accomplished with the help of an IBM 709 computer. A code was developed which takes the data from the multichannel analyzer together with energy calibration data and provides $(d^2\sigma/d\Omega\, d\,E)_{cm}$ vs. E_{cm} and θ_{cm}.

It is seen from Fig. 13-1 that below 7 Mev the proton distributions are anisotropic but symmetric around 90°, and that at higher energies forward peaking becomes increasingly apparent. This peaking is presumably associated with direct interactions. It is relatively less conspicuous for the more proton rich isotopes (Ni^{58}, Ni^{60}) than for the Ni^{62} shown in the figure.

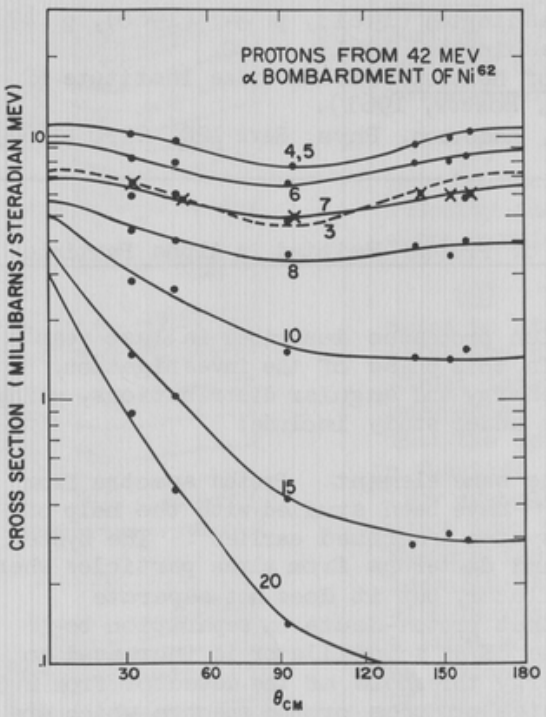

Figure 13-1

Angular distribution of protons from 42 Mev alpha particle bombardment of Ni^{62}.

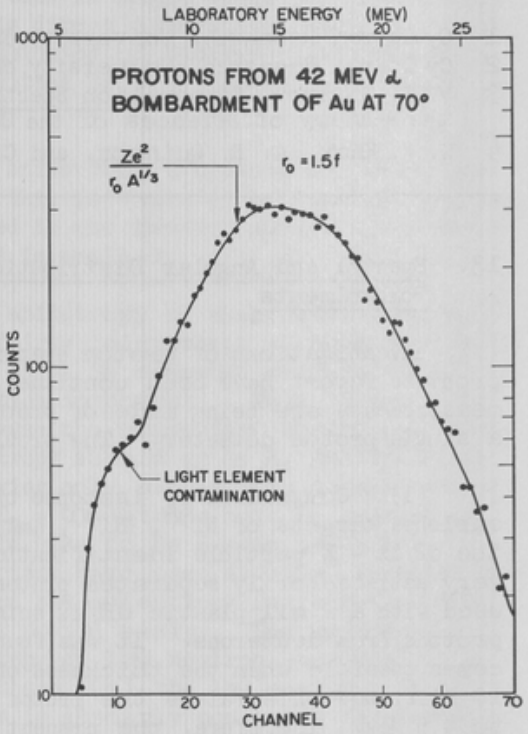

Figure 13-2

Protons at 70° from 42 Mev alpha particle bombardment of gold.

(2) Spectra from heavier elements. The proton yields fall off rapidly as the weight of the target increases, but it was thought desirable to explore some heavy elements, in part to study the low energy portions of the spectra. The low energy part of the spectrum presumably provides a measure of the barrier penetrability for outgoing protons. It is interesting for this reason, in its own right and because a systematic study may help with the determination of the amount of so-called "trapped" protons which appear in the spectra of lighter elements. Some preliminary data from a gold target are shown in Fig. 13-2. Preliminary results have also been obtained for targets in the mass region near silver.

(3) The dependence of spectra on bombarding energy. These measurements have been postponed pending the completion of the energy degrader now under construction. The older degrader system consistently gave rise to excessive backgrounds. (D. Bodansky, I. Halpern, J. Ramus, R. West.)

---

1 Cyclotron Research, University of Washington (1961), p. 53.

---

14. Observation of Pairs of Evaporated Protons

The coincidence studies of pairs of protons evaporated from Ni^{58} bombarded by alpha particles were completed last fall, and have been partially reported. Among the results not as yet reported, are the ones dealing with possible differences in the magnitudes of anisotropies in the angular distributions of successively evaporated protons. In a simple classical model for the evaporation process from a rotating nucleus, the angular distribution of protons with respect to the beam is of the approximate form $1 + x \cos^2 \theta$ where x depends on the nuclear temperature and the moment of inertia. If two protons are emitted in the same reaction, a measurement of their angular distribution provides an average value, $(x_1 + x_2)/2$, of the anisotropy coefficient. It can be shown that a measurement of the angular correlation between the two protons in a plane perpendicular to the beam provides a measure of the product $x_1 x_2$. The results of such a measurement for the protons from Ni^{58} bombarded with 32 Mev alpha particles are shown in Fig. 14-1. They are best fitted with the value $x_1 x_2 = 0.10$; the probable error is about $\pm$ 0.03. This value of $x_1 x_2$ can be combined with the value of $x_1 + x_2$ from an angular distribution study to obtain individual values for x_1 and x_2. The value for $x_1 + x_2$ was determined from a correlation study in a plane containing the beam. The value was 0.79 ± 0.08. As seen from Fig. 14-2, the ratio of x_1 to x_2 lies with reasonably large probability in the neighborhood of 1/3, but there is a good chance that it is as large as 1. If the value of

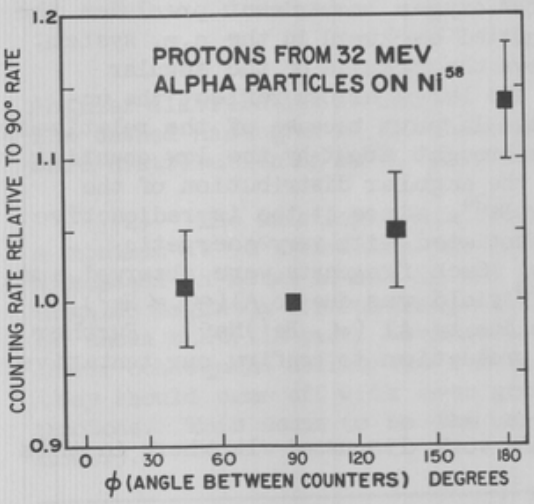

Figure 14-1

Angular correlation between pairs of protons emitted at 90° to the beam and with angle θ between them. The data were normalized to the rate at $\theta = 90°$.

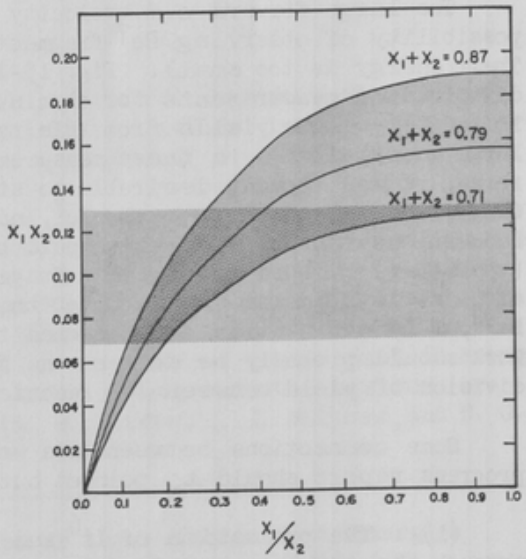

Figure 14-2

Analysis for the values of x (inversely proportional to the nuclear moment of inertia) from a combination of data for angular correlations between emitted protons.

x_1/x_2 is 1/3 it suggests a sizable dependence of the nuclear moment of inertia on excitation energy. This implied dependence disappears as the value of x_1/x_2 increases toward unity. Thus the analysis in Fig. 14-2 suggests but does not establish an energy dependence for the moment of inertia of a rapidly rotating nucleus. (D. Bodansky, C. R. Gruhn, I. Halpern, and R. West.)

15. The Emission of Be^7 from Light Nuclei Bombarded by Helium Ions

The experimental work on the reactions O^{16} (α, Be^7) C^{13} and Al^{27} (α, Be^7) Na^{24} has been completed.[1] It appears that both reactions occur predominantly through the mechanism of compound nuclear formation and decay. This conclusion is supported by the following semiquantitative evidences:

(1) The relative yields of Be^7 from these and a number of other light element targets decrease with A roughly as one would expect on the basis of evaporation theory.

(2) The energies of the Be^7 nuclei, as measured by their ranges, are roughly consistent with expectations based on a statistical model.

(3) The angular distributions of the Be^7 in the c.m. system seems roughly consistent with the expected symmetry around 90°. It should be remarked here that this statement refers to the Al bombardment alone.

The large forward c.m. velocity in the oxygen bombardment precludes the possibility of observing Be^7 fragments emitted backward in the c.m. system. Their energy is too small. Fig. 15-1 shows the results of the angular distribution measurements for aluminum. The large errors reflect the unfortunately lower yields from this target. In part because of the relatively large uncertainties in these measurements brought about by the low counting rates, it was thought desirable to study the angular distribution of the fragment complementary to the Be^7, namely Na^{24}, since it too is radioactive. Backward moving Be^7 fragments would be associated with very energetic ($\sim$ 12 Mev) forward moving Na^{24} fragments. Such fragments were observed and, although it appeared that some of the Na^{24} yield was due to $Al(\alpha, \alpha He^3)$ Na^{24}, a large fraction of it seemed to be due to Al (α, Be^7)Na^{24}. Further work should probably be done on the Na^{24} production to confirm our tentative division of yield between two reactions.

Some connections between this work and work discussed elsewhere in this progress report should be pointed out.

(1) The production of Li^6 and other fragments by 42-Mev alpha particles through the mechanism of direct interactions (Sec. 18). The emission of particles leading to low-lying states in the residual nucleus was examined. It appears that, just as with the emission of lighter particles, like nucleons or alpha particles, the yields to low states can be associated with direct interactions, while the generally more copious yields to higher states have a compound nuclear character.

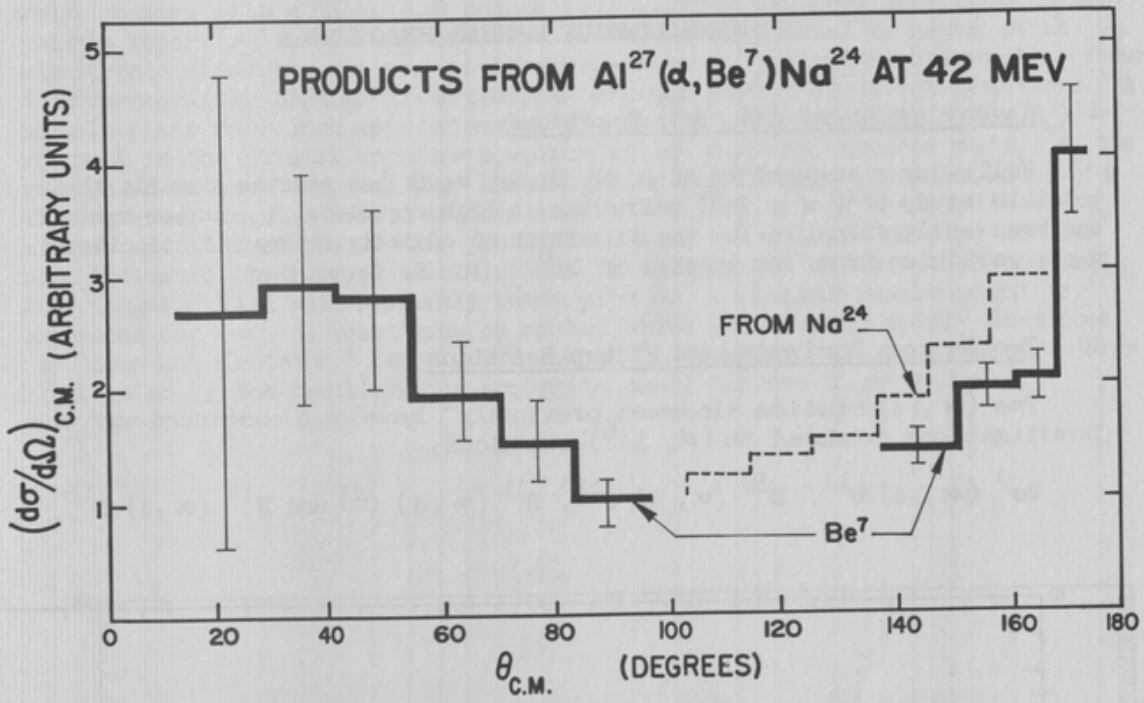

Figure 15-1

Angular distribution of Be^7 in the alpha particle bombardment of aluminum. The dashed histogram is the backward distribution of Be^7 implied by the forward distribution of Na^{24}, corrected for a competing reaction.

(2) The anistropic distribution of the evaporated Be^7 fragments with a minimum at 90° resembles the corresponding curves for protons and neutrons discussed in Secs. 12 and 13 and is no doubt associated with the same angular momentum effects responsible for those anisotropies. Indeed it can be shown that, in part, because of the large mass of the Be^7 nuclei and their consequent ability to remove angular momentum at little cost in energy, they should come off with even greater anisotropies than the neutrons or protons. This seems to be the case. (A. W. Fairhall, I. Halpern, and C. O. Hower).

---

1 C. O. Hower, "The (α , Be^7) Reaction in Light Elements at Energies Below 42 Mev," Ph.D. Thesis, University of Washington, 1962.

---

16. A Review of Compound Nuclear Reactions

A review article on Compound Statistical Features in Nuclear Reactions has been prepared for the Annual Review of Nuclear Science. (D. Bodansky.)

V. MISCELLANEOUS NUCLEAR REACTIONS

17. Investigation of (α, Be^8) Reactions

Following a suggestion of J. S. Blair, work has started towards the possible study of (α, Be^8) reactions in light nuclei. A counter system has been built suitable for the detection of closely separated coincident alpha particles from the breakup of Be^8. (R. E. Brown.)

18. Two Nucleon Stripping and Pickup Reactions

The (α, d) studies discussed previously[1] have been continued and the investigations extended to (α, Li^6) reactions.

Be^9 (α, d) B^{11}, B^{10} (α, d) C^{12}, B^{11} (α,d) C^{13} and N^{14} (α,d) O^{16}

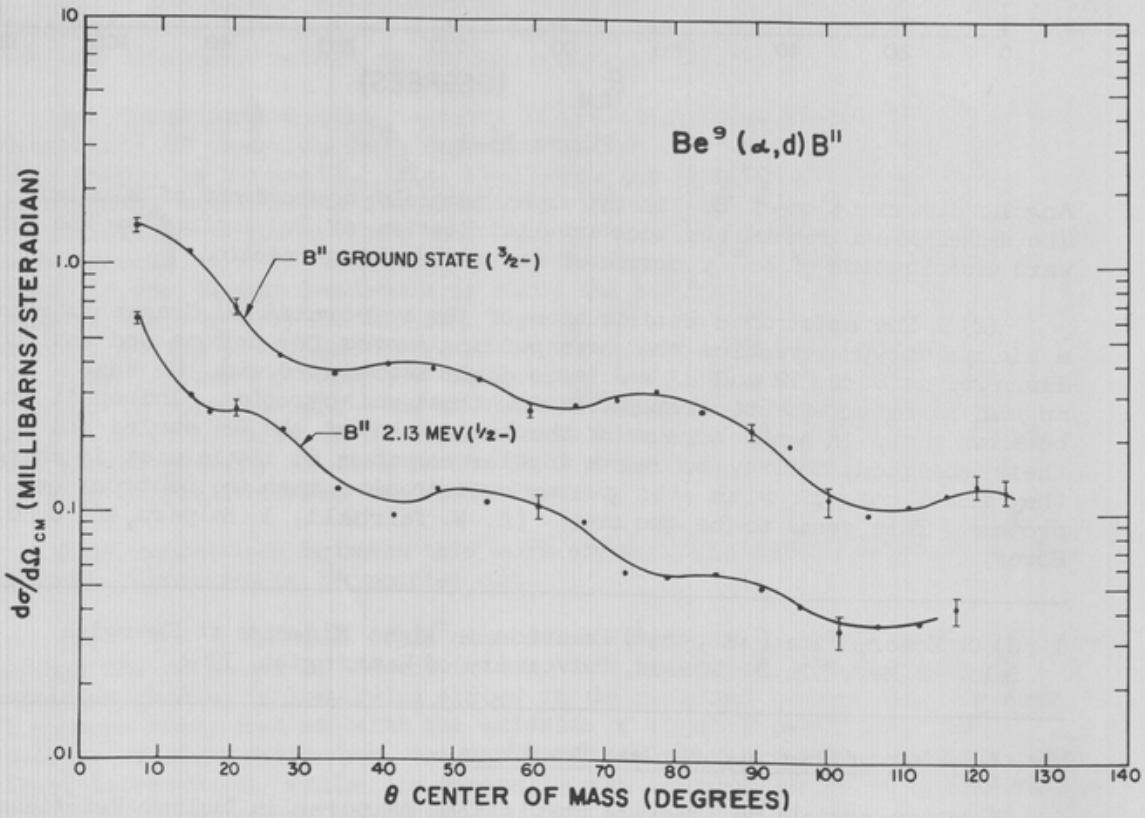

Figure 18-1

Deuteron angular distributions from Be^9 (α, d)B^{11}.

were studied with a dE/dx - E double scintillation counter described in last year's report[2]. Particle identification was accomplished by means of an electronic stretcher and x-y oscilloscope system[3]. These reactions have shown diffraction-like angular distributions characteristic of direct reactions. A simple plane wave Born approximation predicts $d\sigma/d\Omega \propto \Sigma A_\ell J_\ell^2 (q R_o)$ where ℓ is the orbital angular momentum of the captured nucleon pair, R_o the radius of interaction, and A_ℓ the weighting coefficient for each value of ℓ. The observed angular distributions show a "filling in" of the predicted minima and distortions of the predicted maxima. Previous (α, p) results[4] had indicated that strong oscillations in the angular distribution occurred for target nuclei with a weakly bound proton. A similar result might be expected for (α, d) reactions on nuclei which the cluster model[5] describes as "core and deuteron," (e.g., B^{10} and N^{14}). However, as can be seen in Figs. 18-1 to 18-4, the oscillations are quite small for the light targets,

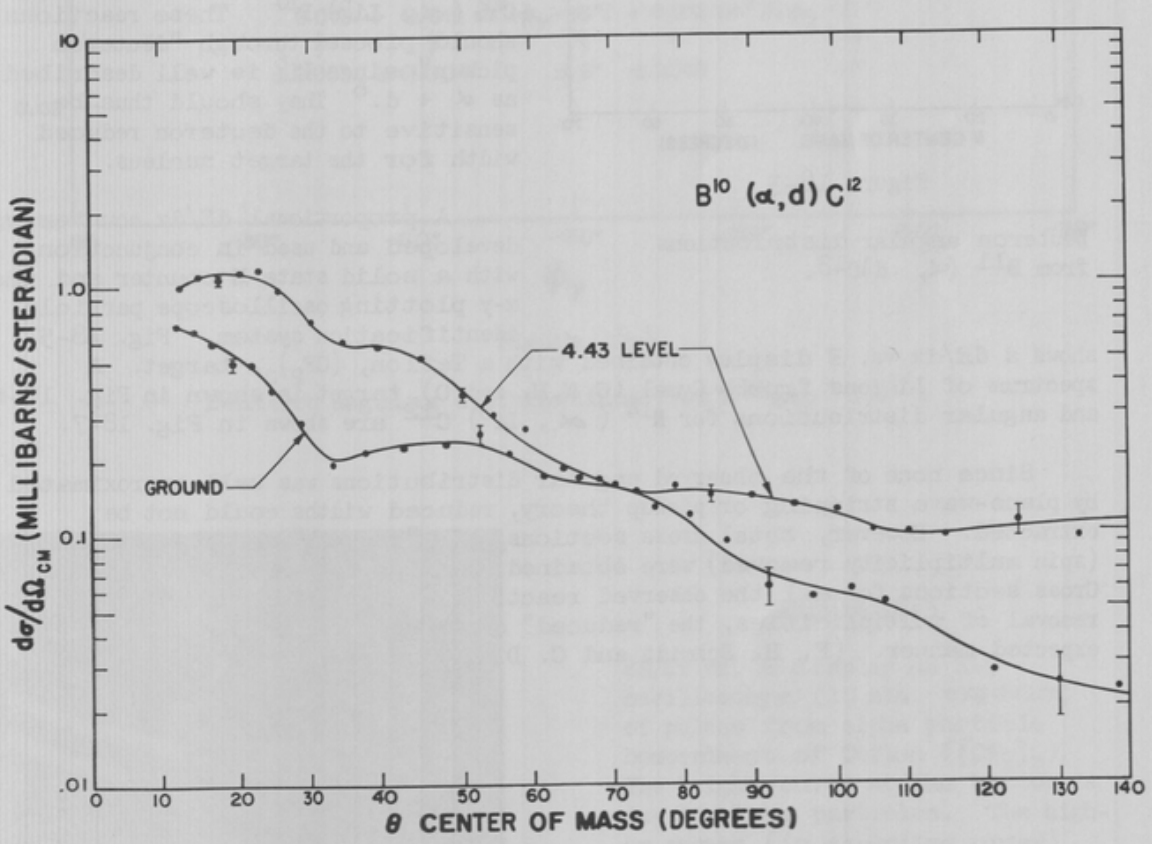

Figure 18-2

Deuteron angular distributions from B^{10} (α, d)C^{12}.

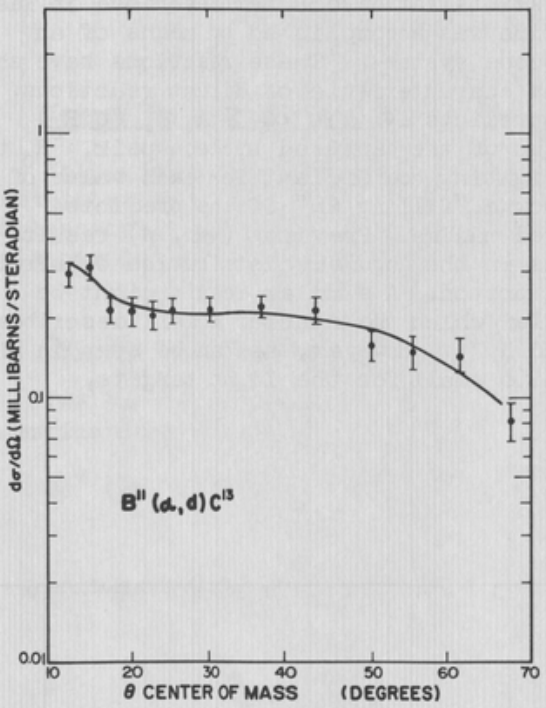

Figure 18-3

Deuteron angular distributions from B^{11} (α, d)C^{13}.

becoming pronounced only for nitrogen. Since it is the surface character of direct nuclear reactions which causes strong interference maxima and minima in the angular distribution, this result can be understood since the light nuclei, through C^{12}, are essentially "all surface."

It would be of greater interest to see if the reduced widths for deuteron clusters increased for nuclei like B^{10} and N^{14}. Since the low-lying levels of interest are bound, a direct interaction must be used to measure these widths. Since an alpha particle is not necessarily well represented as two deuteron clusters, investigations were begun on N^{14} (α, Li^6)C^{12} and C^{12} (α, Li^6) B^{10}. These reactions should proceed through "deuteron pickup" since Li^6 is well described as α + d.[6] They should thus be sensitive to the deuteron reduced width for the target nucleus.

A proportional dE/dx counter was developed and used in conjunction with a solid state E counter and the x-y plotting oscilloscope particle identification system. Fig. 18-5 shows a dE/dx vs. E display obtained with a Teflon, $(CF_2)_n$, target. A spectrum of Li ions from a Cymel (C, N, H, and O) target is shown in Fig. 18-6 and angular distributions for N^{14} (α, Li^6) C^{12} are shown in Fig. 18-7.

Since none of the observed angular distributions was well approximated by plane-wave stripping or pickup theory, reduced widths could not be extracted. However, total cross sections, and "reduced" cross sections (spin multiplicity removed) were obtained from the data (See Table 18-1). Cross sections for all the observed reactions are remarkably similar. After removal of multiplicities, the "reduced" cross sections do vary in the expected manner. (F. H. Schmidt and C. D. Zafiratos.)

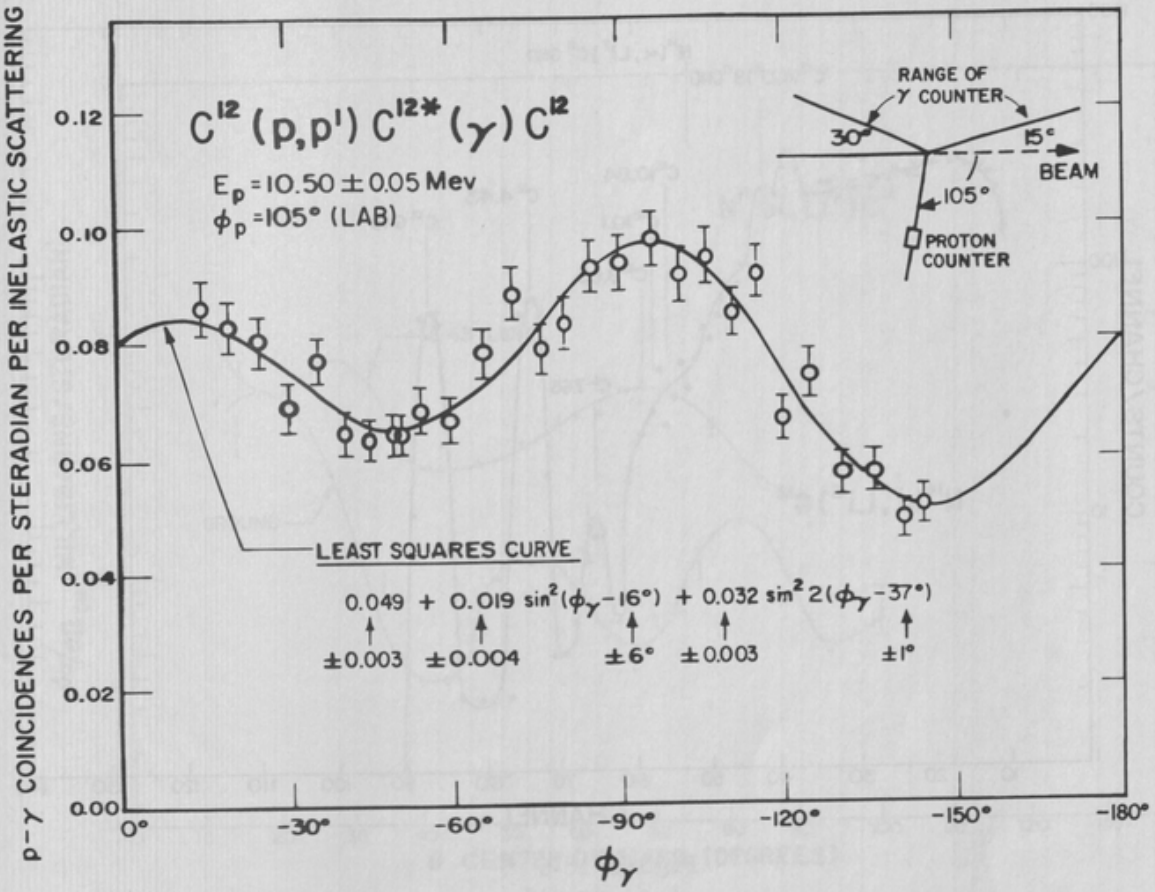

Figure 18-4

Deuteron angular distributions from $N^{14}(\alpha, d)O^{16}$.

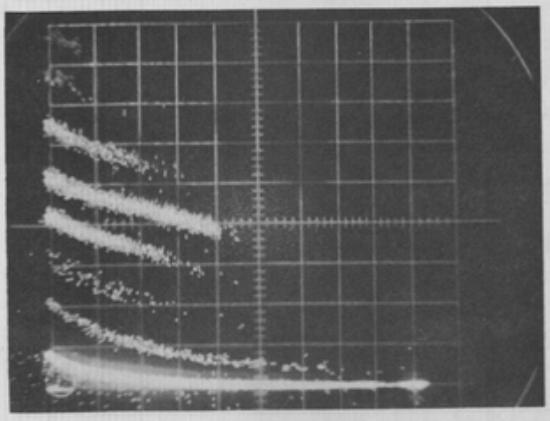

Figure 18-5

dE/dx vs. E display on x-y oscilloscope (10 min. exposure) of pulses from alpha particle bombardment of Teflon ($[CF_2]_n$). The bright curve at the bottom is due to alpha particles. The higher curves (in ascending order) are due to Li, Be, B, C, N, and O.

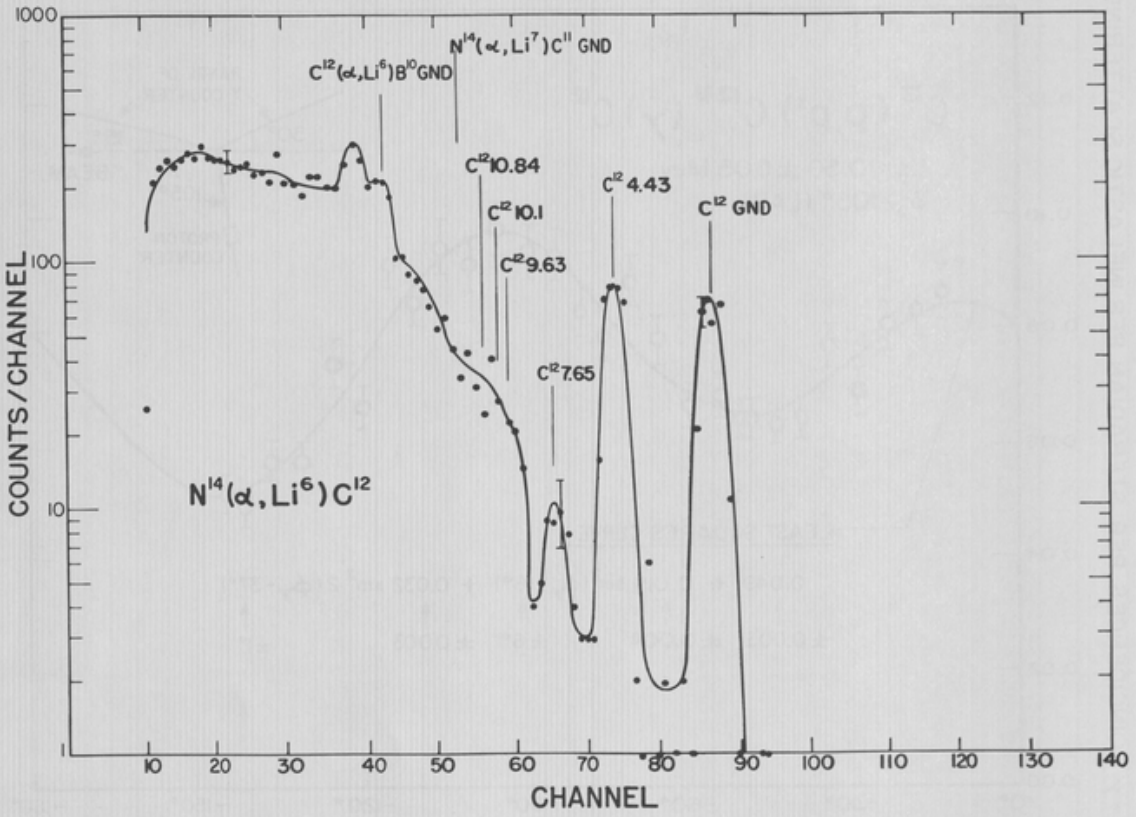

Figure 18-6

Lithium spectrum from Cymel.

Table 18-1. Cross Sections and Reduced Cross Sections

Reaction	σ[a] mb	J_i	J_f	k_i	k_f	N[b]	σ/N mb
$Be^9(\alpha,d)B^{11}$	3.4	3/2	3/2	1.97	1.3	0.66	5.1
$B^{10}(\alpha,d)C^{12}$	1.7	3	0	2.04	1.6	0.11	15
$B^{11}(\alpha,d)C^{13}$	1.25	3/2	1/2	2.08	1.46	0.35	3.4
$N^{14}(\alpha,d)O^{16}$	1.4	1	0	2.21	1.59	0.24	5.8
$C^{12}(\alpha,Li^6)B^{10}$	$\lesssim$1.3	0	3	2.13	1.18	3.9	$\lesssim$0.3
$N^{14}(\alpha,Li^6)C^{12}$	0.83	1	0	2.21	2.14	0.32	2.5

[a] Uncertainties in cross sections $\lesssim \pm$ 30% in all cases.

[b] In plane wave theories $d\sigma/d\Omega \propto N \sum j_\ell (qR_o)$ where $N = (2J_f + 1)k_f / (2J_i + 1)k_i$. J_i and J_f are the initial and final nuclear spins. k_i and k_f are the incident and outgoing wave numbers.

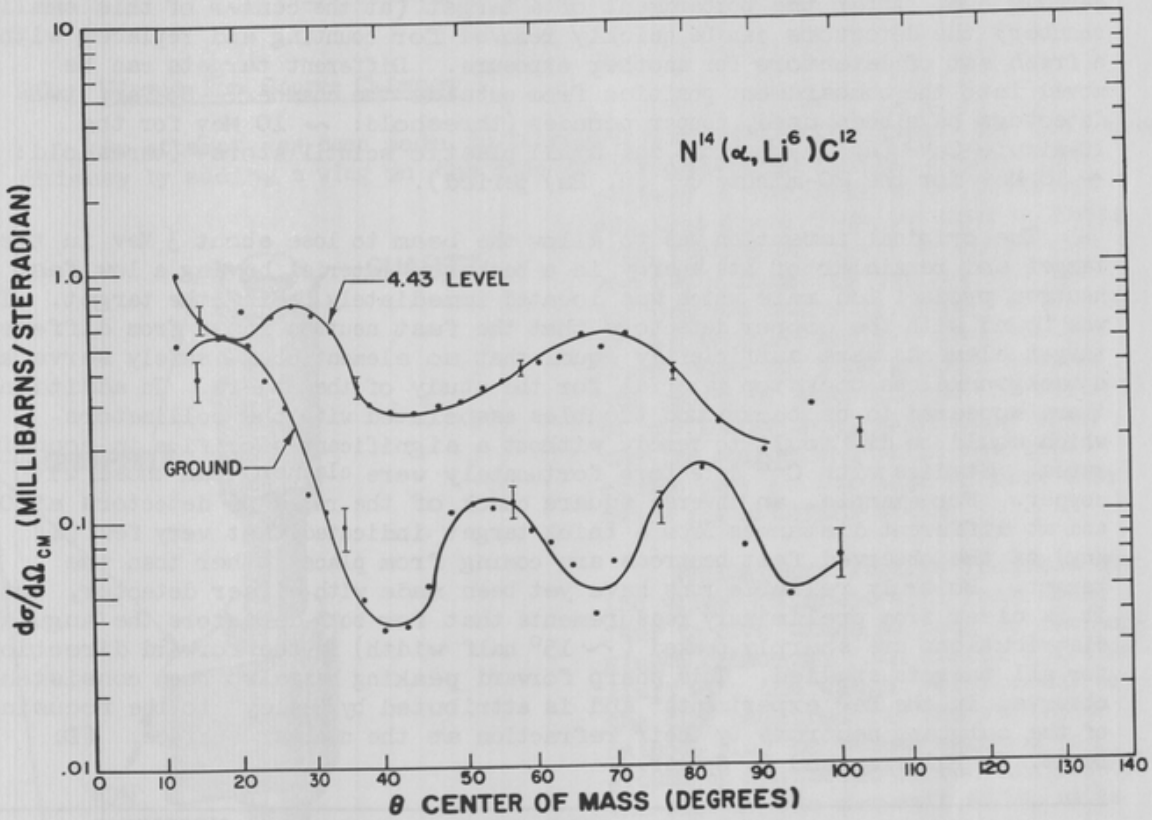

Figure 18-7

Li^6 angular distribution from N^{14} (α, Li^6)C^{12}.

1 Cyclotron Research, University of Washington (1961), p. 40.
2 Cyclotron Research, University of Washington (1961), p. 39.
3 Cyclotron Research, University of Washington (1961), p. 51.
4 Cyclotron Research, University of Washington (1961), p. 38.
5 K. Wildermuth and Th. Kanellopoulos, Nuclear Phys. 7, 150 (1958).
6 M. L. Rustgi, Nuclear Phys. 27, 58 (1961).

19. Angular Distributions of Fast Neutrons in Alpha Particle Bombardments

In order to explore the nature of the reactions which are responsible for the production of fast neutrons in bombardments with alpha particles, it was decided to examine these distributions with the help of threshold detectors. The particular style of measurement was patterned after similar studies being carried out by J. H. Manley at Los Alamos with He^3 ions[1]. The threshold detectors are placed outside a small, thin-walled scattering

chamber[2] which can be attached to our large scattering chamber in place of the Faraday cup. After the bombardment of a target (at the center of this small chamber) the detectors can be quickly removed for counting and replaced with a fresh set of detectors for another exposure. Different targets can be moved into the bombardment position from outside the chamber. So far, two detectors have been used, copper pennies (threshold: $\sim$ 10 Mev for the 10-minute Cu^{63} (n, 2n) period) and small plastic scintillators[3] (threshold: $\sim$ 18 Mev for the 20-minute C^{12} (n, 2n) period).

The original intention was to allow the beam to lose about 3 Mev in the target and remainder of its energy in a backstop material having a low fast neutron product ion rate which was located immediately behind the target. It was found with the copper detectors that the fast neutron rates from different target elements were sufficiently equal that no element could safely serve as a backgroundless backstop material for the study of the others. In addition, there appeared to be background troubles associated with the collimators which would be difficult to remedy without a significant sacrifice in counting rates. Studies with C^{12} detectors fortunately were cleaner than those with copper. For example, an inverse square check of the rates of detectors at 0^{o} and at different distances from a thick target indicated that very few (if any) of the observed fast neutrons are coming from places other than the target. No truly reliable runs have yet been made with either detector, but it is clear from preliminary measurements that for both detectors the angular distributions are sharply peaked ($\sim 15^{o}$ half width) in the forward direction for all targets studied. This sharp forward peaking has also been consistently observed in the He^{3} experiments[1] and is attributed by Henley[4] to the focusing of the outgoing neutrons by their refraction at the nuclear surface. (D. Drake, I. Halpern, and R. Spiger.)

---

1 J. H. Manley, Bull. Am. Phys. Soc. II, 7, 270 (1962).
2 This chamber was kindly loaned to us by the Los Alamos Scientific Laboratory.
3 The counting rates with these detectors are relatively high because the β radiation can be efficiently counted with a photo-tube. The use of these detectors was suggested to us by Dr. R. B. Day.
4 E. M. Henley, (private communication).

20. Winged Ion Source Chimney

An attempt has been made to increase the useful lifetime of the ion source chimney by adding a wing on the side of the chimney (see Fig. 20-1). The purpose of the wing is to intercept all ions drawn from the source during that portion of the r.f. cycle when the dee voltage is too low and the initial ion phase is wrong for acceleration to full radius. Removal of these unwanted ions greatly reduces the amount of sparking in the vicinity of the ion source, especially after the ion source exit slit has been eroded away at its edge to more than twice its original width.

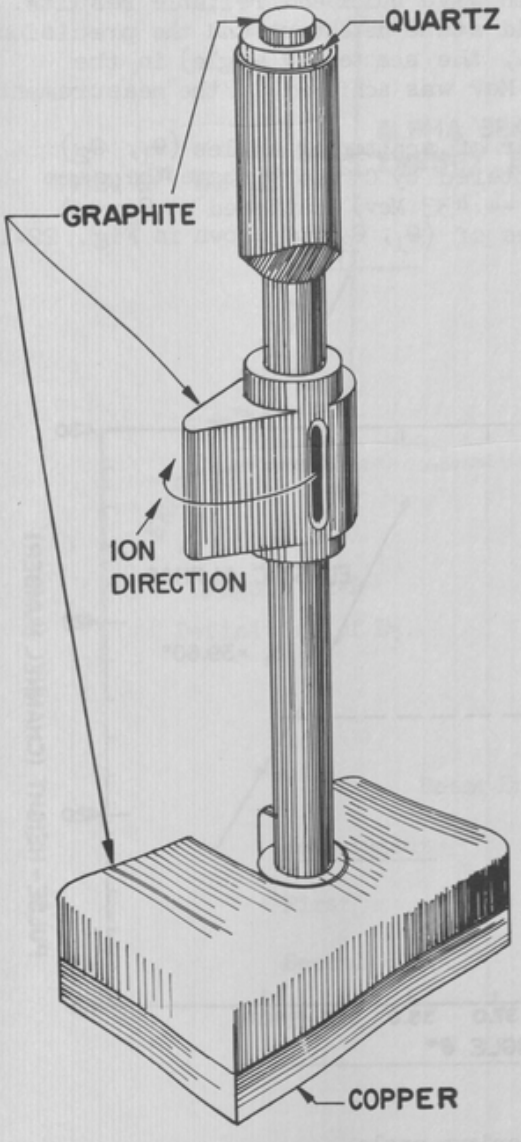

Figure 20-1

Winged ion source chimney.

Preliminary results indicate that the winged chimneys will last about four to five times as long as the non-winged chimneys. The useful lifetime limit with the winged version may be the time required for the reflector cathode plug to become shorted to ground by sputtered carbon instead of the size of the ion exit slit, as is the case with the plain chimneys. (T. J. Morgan.)

21. Vacuum Test Chamber.

A self-contained vacuum chamber has been constructed in order to facilitate testing of scintillation counters and solid state counters in vacuum, to permit targets to be prepared and transferred to the 60-inch scattering chamber in vacuum, and for other reasons. The vacuum box is 18 inches high, 18 inches deep and 24 inches long and is accessible by a door covering one entire side, and four ports identical to those in the 60-inch scattering chamber. Low voltage leads have been brought into the vacuum and provision is made to introduce high voltage and signal leads through interchangeable ports.

The vacuum is maintained by a 90 liter/second air cooled diffusion pump and a permanently mounted 2 cu. ft./min. Kinney pump. The pressure is monitored by thermocouple gauges and an ion gauge. Vacuums of the order of 2 to 3×10^{-5} mm Hg have been maintained. (D. L. Hendrie and T. J. Morgan.)

22. Beam Energy Measurement

A simple method of measuring the energy of the collimated alpha beam in the 60-inch scattering chamber was found to give quick and reliable results. Because of the enhanced resolution of solid state detectors and the precision control of the detector arm position (i.e., the scattering angle) in the scattering chamber, an accuracy of ± 0.25 Mev was achieved in the measurement.

The method[1] consists of finding a pair of scattering angles (θ_1, θ_2) such that alpha particles elastically scattered by C^{12} at θ_1 have the same pulse height as the inelastic alphas (Q = -4.433 Mev) scattered at θ_2. A typical experimental curve providing values of (θ_1, θ_2) is shown in Fig. 22-1.

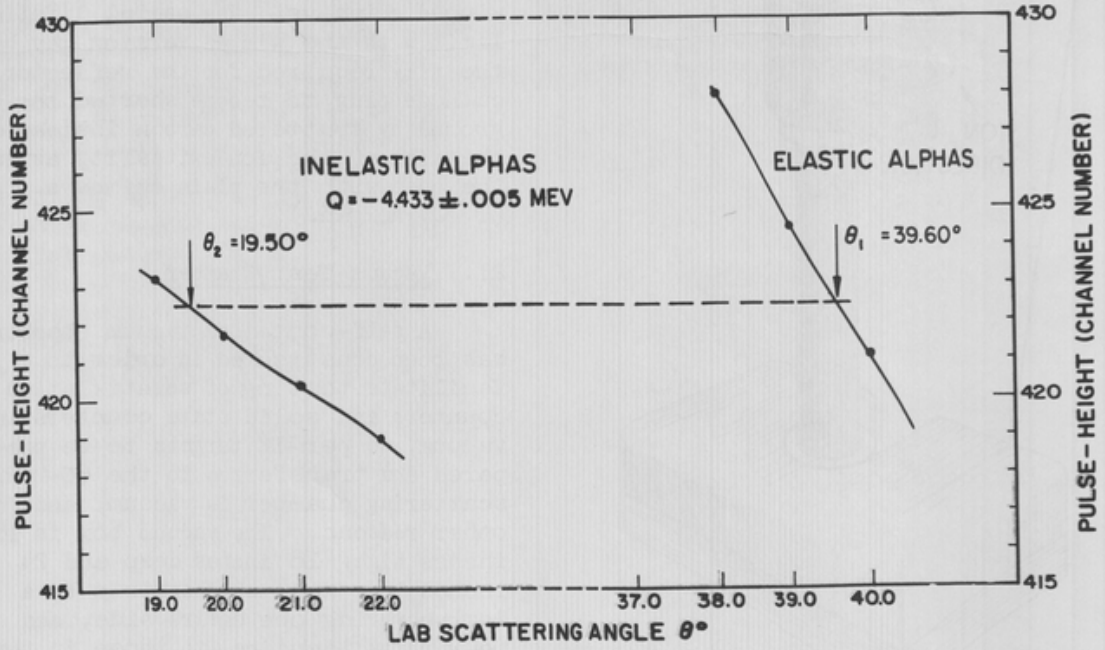

Figure 22-1

Pulse height vs. scattering angle.

For each pair (θ_1, θ_2) we have the equality,

$$E_3\ (Q = 0,\ \theta = \theta_1,\ E_1) = E_3\ (Q = -4.433,\ \theta = \theta_2,\ E_1),$$

which can be solved numerically or graphically, yielding the beam energy E_1. (E_3 is defined in Fig. 22-2.)

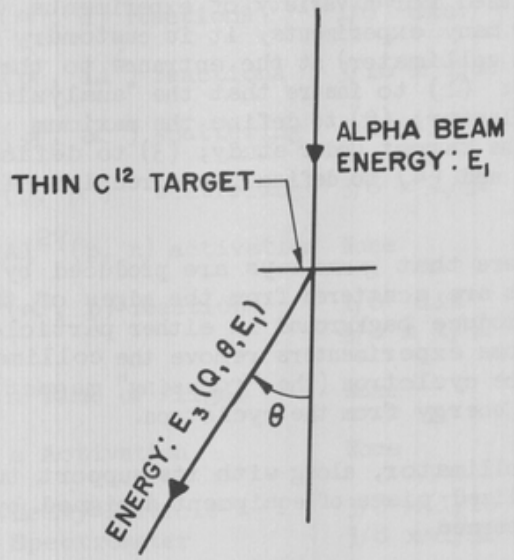

Figure 22-2
Definition of E_3.

The estimated error associated with the measurement is ± 0.250 Mev. This is due mainly to the uncertainty in the scattering angles (± 0.05°) and in the known[2] value of Q ($Q = 4.433 \pm 0.005$ Mev).

The energy measurement was repeated three times over a period of three months under the same conditions of tight beam collimation and duct slit position. The results are shown in Table 22-1.

Table 22-1

Beam Energy Measurements

Measurement	E_1 (Mev)
First	42.03 ± 0.25
Second	41.94 ± 0.25
Third	41.98 ± 0.25
Average	41.98 Mev

Using a similar method, the proton beam energy, under the same conditions, was found to be 10.47 ± 0.05 Mev. (I.M. Naqib and D. C. Shreve.)

1 Suggested by D. Bodansky.
2 F. Ajzenberg-Selove and T. Lauritsen, Nuclear Phys. 11, 116 (1959).

23. Range of Beam Magnitudes and Physical Dimensions Used in Scattering Chamber Experiments

The 60-inch scattering chamber is used for a variety of experiments under widely differing conditions. For many experiments, it is customary to place a set of beam delimiting slits (a collimator) at the entrance to the chamber. The role of the collimator is: (1) to insure that the "analyzing" magnet is operating as a beam energy selector; (2) to define the maximum divergence angle of the beam striking the target under study; (3) to define the position of the beam on the target; and (4) to define the direction of the beam center line.

The chief evils of the collimator are that gamma rays are produced by the beam striking it, and that particles are scattered from the edges of the collimator slits. Both phenomena can produce background in either particle or gamma ray detectors. Accordingly, some experimenters remove the collimator, and rely upon the first magnet beyond the cyclotron (the "focusing" magnet) and the duct slit to select the desired energy from the cyclotron.

Generally speaking, a particular collimator, along with its support tube and any internal shielding, is a specialized piece of equipment designed by and used by the individual or group concerned.

In order to learn what were the practices adopted in various experiments, a survey was made of beams and collimators in use during the past year. The results of this survey are listed in Table 23-1. The most striking feature is the great range of beam magnitudes used, viz., from 0.1 to 200 mμa with collimators, and up to 2μa without, or variation of a factor of 2×10^4. The lower limit of beams desired is generally set by counting rate, or pile-up considerations. The second feature is that most experimenters believe they could profit by a higher upper limit, particularly those using the heavy particle spectrometer. The maximum beams listed are thus more often limited by the cyclotron and external beam system than by the experimental conditions. It is also worth noting that the mechanical feature built into the 60-inch scattering chamber, which permits easy alteration from one collimator tube to another (or to none), has provided the flexibility in individual experiments required for the multiple uses to which the chamber has been put. (F. H. Schmidt.)

Table 23-1

Survey of Beams and Collimators Used in Experiments

Carried Out in 60-inch Scattering Chamber

Experiment	Collimator*	Beam - mμa			Is Maximum Sufficient?
		Min.	Max.	Av.	
(α, d) reactions	1/8" dia.	0.1	30	10	Yes
(α, Li^6) reactions	3/16 x 1/16	0.1	20	8	No
(α, α') scattering	3/8 x 1/32	10	60	30	No
(p, p') scattering	3/8 x 1/32	10	50	30	No
$Al^{27}(p, n)$ activation	None	500	2000	1500	No
(α, p) reactions	1/8" dia 3/8 x 1/32	0.2 0.2	90 50	10 10	No
n Time of Flight	None	50	100	-	No
n Activation	None	200	500	-	No
Heavy Particle Spectrometer	3/8 x 1/16 3/8 x 1/32	40	200	75	No
$(\alpha, \alpha' \gamma)$ Angular Correlations	None	1	20	5	Yes
$B^{10}(p, n)C^{10}$ Activation	None	20	1500	300	No
$(\alpha, \alpha n f)$ reactions	1/8" dia.	0.5	100	20	Yes
$(p, p' \gamma)$ Angular Correlations	None	1	20	7	Yes

*Individual differences, such as provisions for shielding, divergence angle, "cleanup" slits, etc. are not reflected in this tabulation.

24. Three-Stage Tandem Van de Graaff Program

In the middle of November we received a grant of $1.24 million from the National Science Foundation for the purchase of a Tandem Van de Graaff Accelerator. The remainder of the funds for the projected full three-stage accelerator will be granted, it is expected, during the next fiscal year.

Contract negotiations with the High Voltage Engineering Corporation were successfully completed during the first week in January, at which time a contract was signed for the construction of a type FN, 15 Mev, tandem machine. The contract contains price options for the injector stage and auxiliary equipment which are good until November 1, 1962.

Design studies for the building to house the accelerator and to provide the necessary ancillary laboratory, office, and other space were carried out by our own personnel during the fall months. After the grant was received, the University Board of Regents appointed the architectural firm of John Graham and Son to proceed with the building designs. Since then we have been working closely with representatives of this firm, and the final plan for the building was crystalized in April. The design was accepted by the University Architectural Commission and approved by the Regents at their April meeting. John Graham and Son are now proceeding with the working drawings. It is expected that the plans will be submitted for bids in June, and construction will begin in late August or early September.

The projected building, as shown in Fig. 24-1, is contiguous to the present cyclotron building. It features ample space for electronic counting equipment and future computer installation. Every effort was made to put the shielded experimental areas close to both the counting areas and to test set-up areas. The natural contours of the site were utilized to the fullest to provide radiation shielding.

The tandem stage will be delivered in the fall of 1963. We hope to start performing experiments with this stage by the spring of 1964. (T. J. Morgan and F. H. Schmidt.)

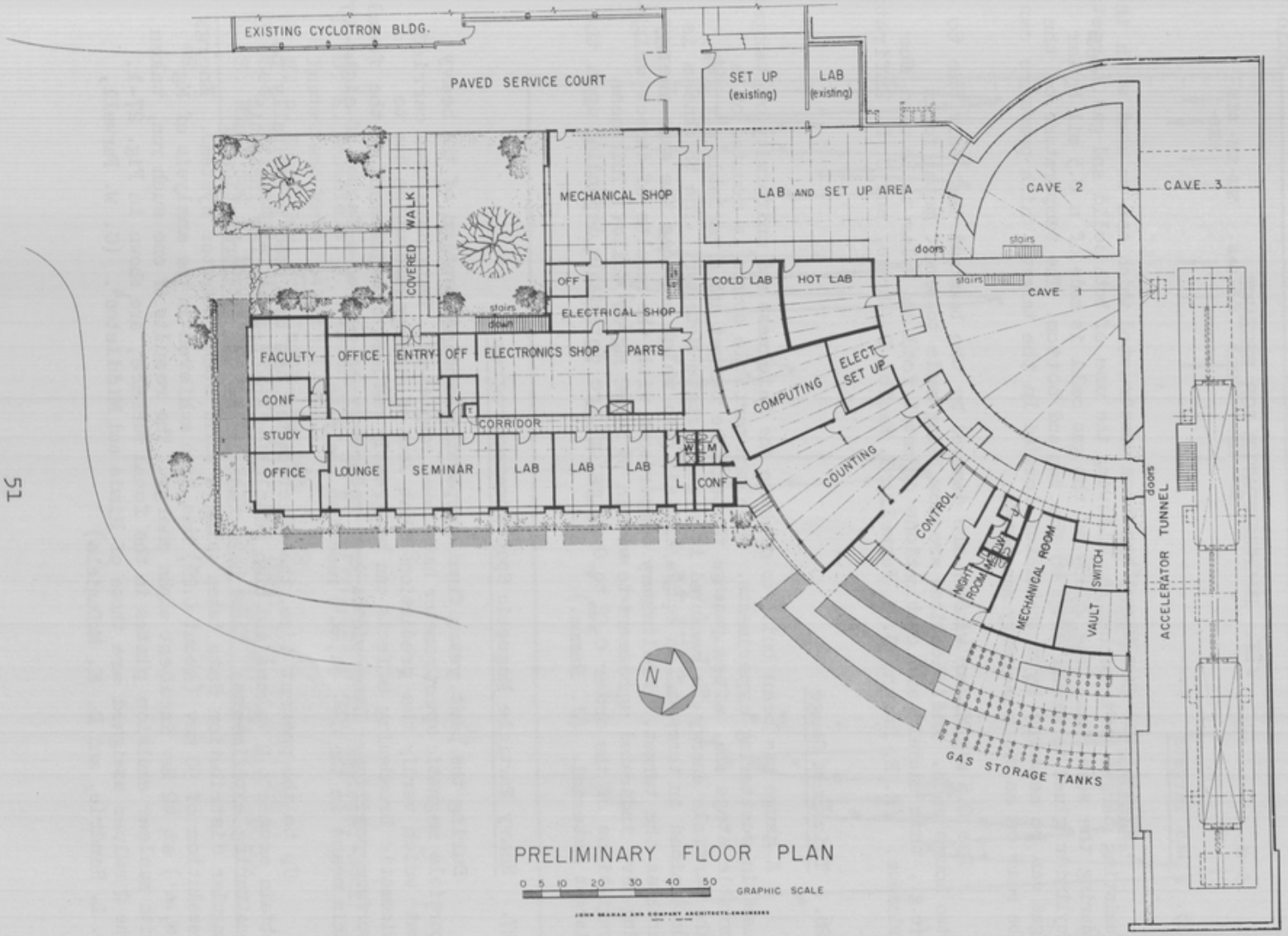

Figure 24-1

Plan for projected three-stage tandem Van de Graaff laboratory.

VII. INSTRUMENTATION FOR RESEARCH

25. Gas Targets

A cylindrical gas target has been constructed which can be used with the existing target lift mechanism, allowing the use of both solid and gas targets during the same run. The window of the gas cell is made of a 0.5 mil Mylar cylinder glued to brass rings on the top and bottom. The temperature of the gas can be measured by a thermistor located in the target, while pressure can be read on an 80 cm mercury manometer.

The 0.5 mil Mylar windows are damaged by the beam and last only one to two hours each. Modifications are now being made to permit metal foils (e.g., thin nickel) and combinations of metal foil and Mylar to be used for windows. (R. E. Brown, G. W. Farwell, I. Naqib, D. Shreve, and C. D. Zafiratos.)

26. Thickness Gauge

A gauge has been built to measure the thickness and uniformity of targets used in scattering experiments. An alpha particle source is mounted on a movable stage and, after passage through the target and a variable air gap, the particle energy is measured in a solid state detector. The thickness is determined in terms of an equivalent air path which produces the same energy loss as the target. Preliminary comparisons with the results of direct weighing have indicated agreement to within 5% for 2 mg/cm^2 foils. Thickness variations of the order 0.02 to 0.05 mg/cm^2 are detectable depending upon the target material. (J. Ramus.)

27. Heavy Particle Magnetic Spectrometer Program

During the past year, final preparation and calibration of the heavy particle magnetic spectrometer have been completed. Tests have been carried out[1] which verify the prediction[2] that loss of energy resolution due to kinematic broadening effects can be greatly reduced by adjustment of the focal surface position. Line widths were reduced by as much as a factor of eight by this means in the C^{12} (α, α') reaction analysis.

Up to the present time, the spectrometer has been used principally to obtain accurate Q values and high resolution spectra in a few inelastic scattering experiments; these have facilitated the interpretation of angular distribution data taken using a solid state detector system[3]. Energy resolution of 90 kev (about 0.2%) has been achieved in the analysis of Mg^{24} (α, α') at 42 Mev incident alpha energy. The results of one such run, taken with nuclear emulsion plates in the focal surface, are shown in Fig. 27-1. The Q values assigned are those of Hinds and Middleton[4]. (G. W. Farwell, D. L. Hendrie, and D. K. McDaniels.)

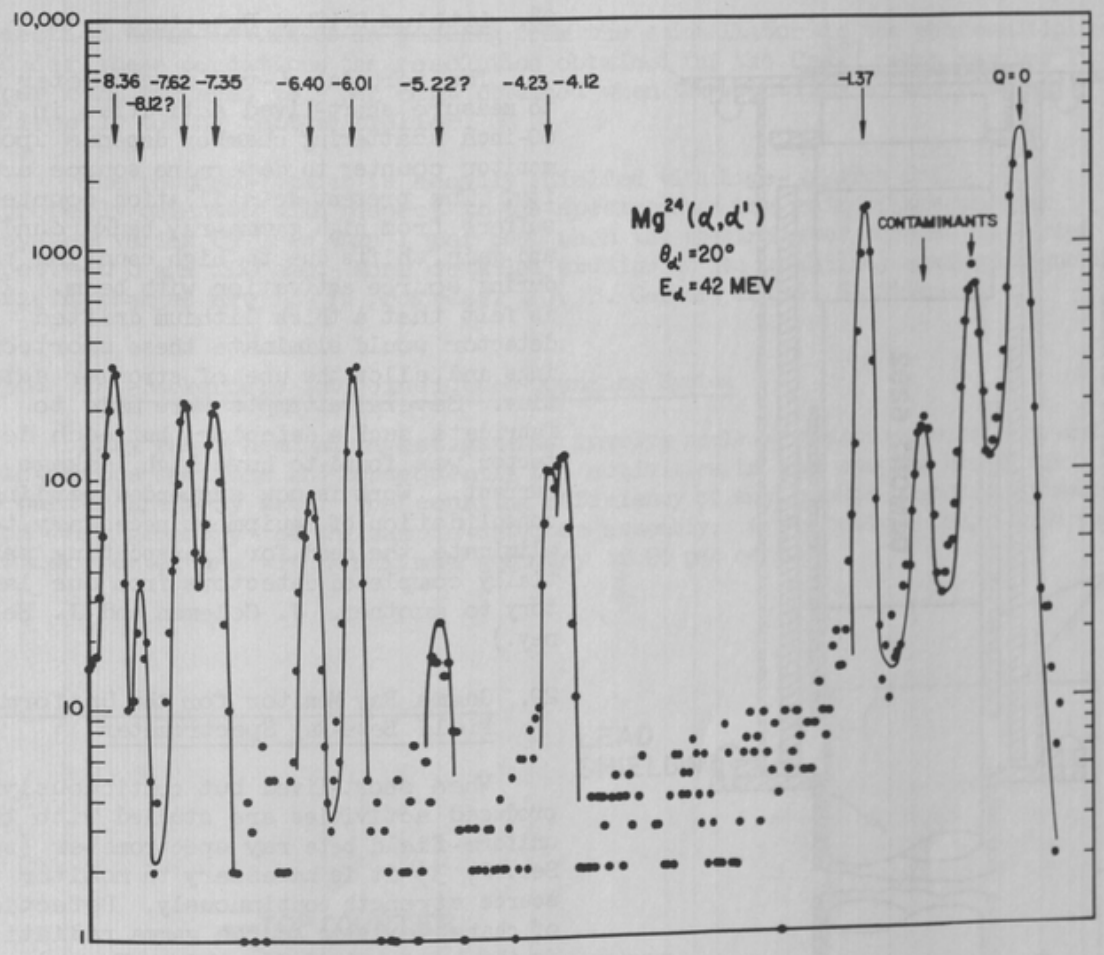

Figure 27-1

Magnetic analysis of particles from $\alpha + Mg^{24}$.

1 D. K. McDaniels, W. Brandenberg, G. W. Farwell, and D. L. Hendrie, Nucl. Instr. and Meth. 14, 263 (1961).
2 H. A. Enge, Rev. Sci. Instr. 29, 885 (1958).
3 See, for example, I. M. Naqib, Bull. Am. Phys. Soc. 7, 73 (1962).
4 S. Hinds and R. Middleton, Proc. Phys. Soc. (London) 76, 553 (1960).

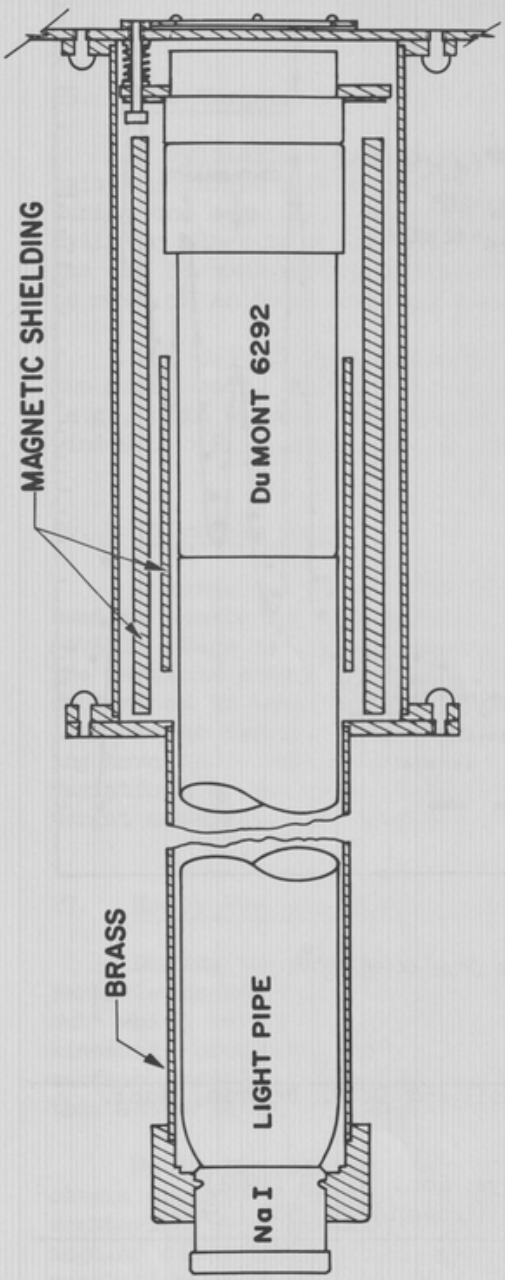

Figure 29-1

Cross section of gamma-ray monitor counter. The length of the light pipe is four feet.

28. Lithium Drifted Detectors

The toroidal β-ray spectrometer used to measure short-lived activities in the 60-inch scattering chamber depends upon a monitor counter to determine source activity. The present scintillation counter suffers from high gamma-ray background and gain shifts due to high counting rates during source activation with beam. It is felt that a thick lithium drifted detector would eliminate these shortcomings and allow the use of stronger activities. Several attempts were made to fabricate such a detector, but each detector was found to have high leakage current. Work is now suspended pending consolidation of equipment necessary to eliminate the need for transporting partially completed detectors from one laboratory to another. J. Coleman and J. Heagney.)

29. Gamma Ray Monitor for the Uniform Field Beta-Ray Spectrometer

When short-lived but continuously produced activities are studied with the uniform-field beta ray spectrometer (see Sec. 2, 3) it is necessary to monitor the source strength continuously. Detection of characteristic source gamma radiation is the best method for this. However, to do so requires a gamma ray counter which has both good resolution and which is insensitive to strong and variable magnetic fields.

A gamma-ray monitor has been constructed for use with the uniform field beta-ray spectrometer which consists of a 1.5-in. dia. x 1-in. NaI (Tl) scintillator coupled to a DuMont 6292 photomultiplier through a four-foot light guide (see Fig. 29-1). To obtain the greatest possible light collection, the light guide was made of ultraviolet-transmitting Plexiglass. The light guide was polished and mounted so that its carefully cleaned surface is in contact only with the scintillator housing and the photomultiplier, and was shaped so that the cross

section never decreases in passing from the scintillator to the photomultiplier. Under these conditions the resolution obtained for the Cs^{137} gamma ray was 11 per cent compared to 9 per cent obtained when the scintillator was coupled directly to the photomultiplier.

The photomultiplier is heavily shielded with high-μ iron foil. When properly oriented with respect to the spectrometer the gain of the monitor system varies by less than 1 per cent when the spectrometer current is varied between 0 and 100 amp. More detailed studies of its stability against magnetic field changes are now in progress. (J. B. Gerhart and G. S. Sidhu.)

30. Low-Background Anticoincidence Counting System

Many radiochemical investigations involve nuclear reactions with extremely low cross sections and consequently the activities in the samples which are counted are very weak. The counting efficiency of any counter depends primarily on the "geometry" of the sample-detector assembly. Previously we have used end-window detectors with a maximum geometry of 20 per cent.

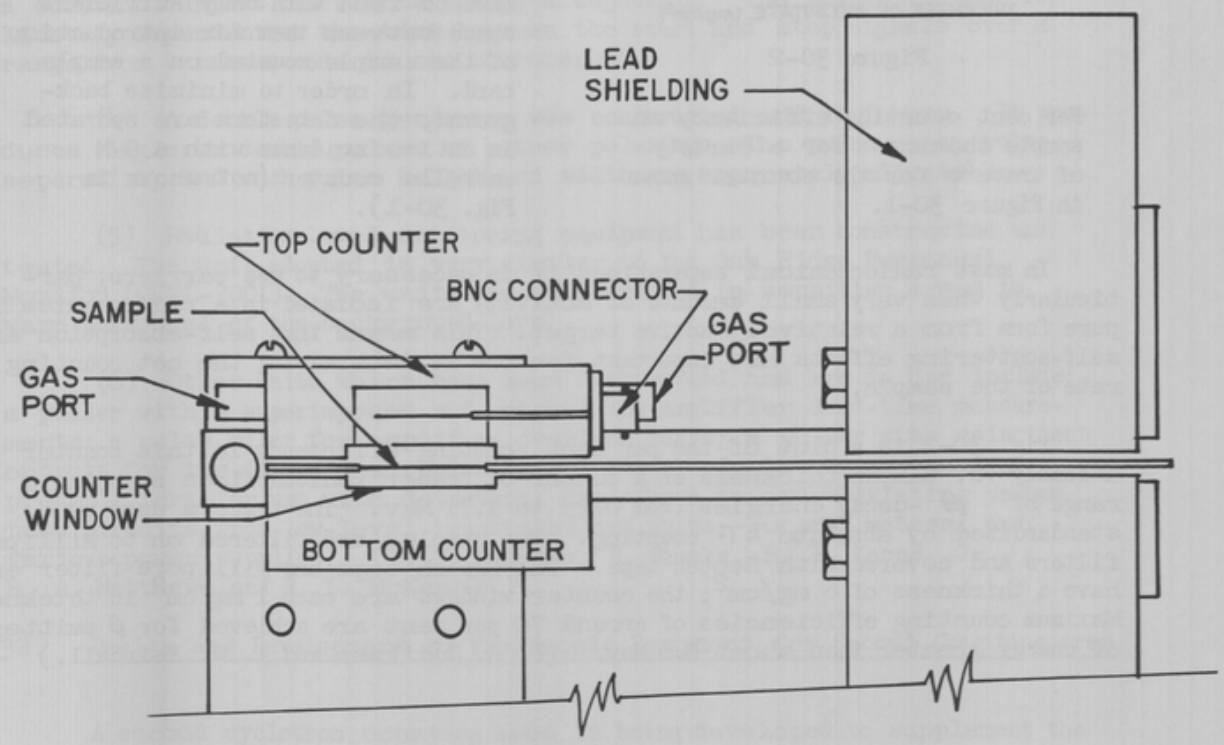

Figure 30-1

Low background anticoincidence counter.

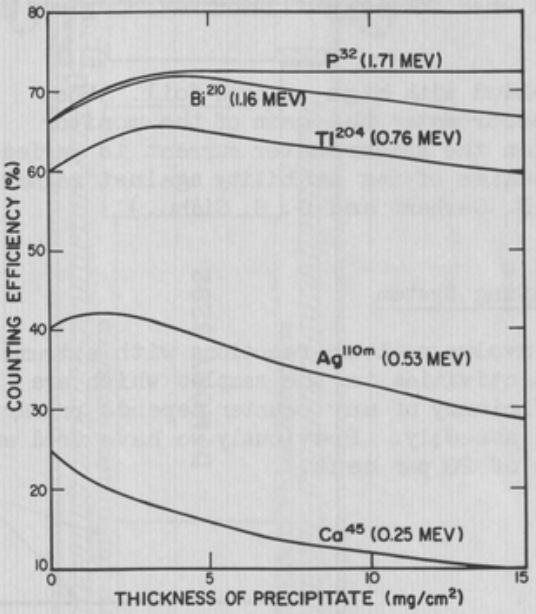

Figure 30-2

Per cent counting efficiency vs. sample thickness for a variety of tracers for the counter shown in Figure 30-1.

Another factor related to the determination of accurate decay curves is the background which is present in our counters. The gain in precision of counting is proportional to the decrease in background which can be affected.

In order to have maximum counting efficiency it is necessary to count weightless samples in a 4π counter. There are several practical drawbacks to this, however, and we have compromised instead on a system which approximates 4π geometry but which will handle samples of finite thickness and does not require the elaborate mounting and sample introduction techniques of true 4π counting. This system, shown in Fig. 30-1, uses two thin end-window counters face to face with only sufficient space between them for introduction of the sample mounted on a sample card. In order to minimize background, the detectors are operated in anticoincidence with a G-M umbrella counter (not shown in Fig. 30-1).

In most radiochemical separations it is necessary to use carriers, particularly when very small amounts of activity are isolated in a radiochemically pure form from a relatively active target. This means that self-absorption and self-scattering effects are important factors in determining the net counting rate of the sample.

Fig. 30-2 is a plot of the per cent counting efficiency in this counter assembly vs. sample thickness of a number of tracer radionuclides spanning a range of β -decay energies from 0.25 to 1.75 Mev. The tracers used were standardized by absolute 4π counting. The samples are filtered on to Millipore filters and covered with Scotch tape. The Scotch tape and Millipore filter each have a thickness of 6 mg/cm^2; the counter windows are each 1 mg/cm^2 in thickness. Maximum counting efficiencies of around 70 per cent are achieved for β emitters of energy greater than about 0.8 Mev. (P. H. Gudiksen and A. W. Fairhall.)

31. Design and Development of Electronic Equipment for Current Use

Electronic equipment built for the existing counting area or general laboratory use is described in the following paragraphs. Equipment for the new second counting area is described in Sec. 32.

(1) Gating signals for the commercial 512-channel analyzer and the associated storage units are provided by a new slow coincidence chassis. This unit provides two independent coincidence outputs from any combination of three input signals (taken all together, two at a time, or singly). The outputs are biased correctly for the multichannel analyzer. Additional outputs are provided to drive scalers or other equipment either from the individual channels or from the coincidence signals.

(2) A paper tape perforator, a paper tape reader, and a transfer chassis to drive a typewriter from paper tape were purchased and installed for use with the 512-channel analyzer.

(3) A new time-to-pulse-height converter was constructed and tested, and is in use. Results with this unit are superior to those obtained with a previous vacuum tube version. The circuit consists basically of a very fast binary circuit, which controls a transistor switch which in turn allows a constant current circuit to charge a capacitor. The output voltage is linearly dependent on the time between the start and stop signals over a range from 4 nanoseconds to one microsecond.

(4) A double pulse generator was constructed and is in use. It produces single or double pulses of either polarity. The pulse rate, pulse separation, and each pulse height and width are separately adjustable.

(5) Radiation level monitoring equipment has been constructed and tested. The unit adopted is very similar to the Oak Ridge Personnel Monitor (ORNL-3001). The units are to be placed in sensitive areas to warn personnel of the background level.

(6) Other units which have been constructed and are in use include: a pulser with a superimposed r.f. signal for amplifier dead-time measurements; a pulse mixer for amplifier overload tests; a pulser with coincident outputs for two-dimensional pulse height tests; single channel analyzers; preamplifiers for use with detectors; amplifiers to drive existing vacuum tube circuits from low-level transistorized units; control meters; and various power supplies. (L. H. Dunning, H. Fauska, R. E. Karns, Jr., R. A. Matthews, and R. L. McKenzie.)

32. Design and Development of Electronic Equipment for Second Counting Area

A second cyclotron counting area is being developed to supplement the existing counting room. This will make it possible for two groups to use or test electronic equipment simultaneously. In developing equipment for the second counting area, transistor circuitry and printed card construction

techniques are being used whenever possible. The latter feature will facilitate the duplication of units for future use with the tandem Van de Graaff accelerator.

Specific units which have been built for use in the second counting area include:

(1) Several six-decade decimal scalers. Each decade is on a newly designed printed circuit card, which uses nixie readout and also has provision for analog and coded decimal outputs. The scalers can be started and stopped by a remote control unit, and can be gated by an external pulse.

(2) A scaler control unit, which can simultaneously start and stop up to twenty external scalers, current integrators, or pulse height analyzers. A photograph of this unit is shown in Fig. 32-1. The counting is started manually, and can be stopped either manually or on the basis of a predetermined count or a predetermined time. The impulses for the predetermined count are accumulated in a six-decade decimal scaler, of the type described in the previous paragraph. The input for this scaler may come from an external signal (for "predetermined count" operation) or from internal scaling of 60 cps power (for "predetermined time" operation). The time is independently monitored in a five-decade nixie readout scaler which displays time to the nearest 0.1 sec or 0.01 minute. An audible signal is also provided from the predetermined count unit, to aid the experimenter in noting sudden changes in counting rates (in the absence of audible counting registers).

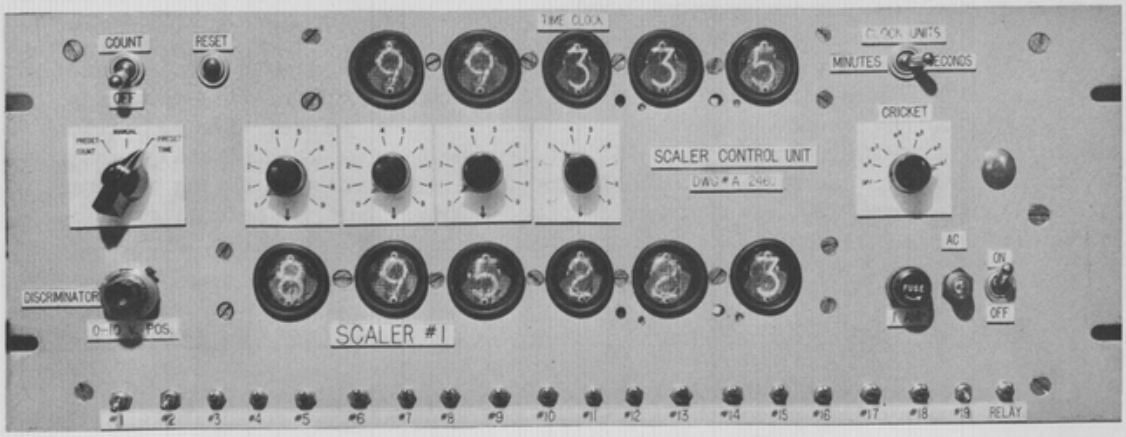

Figure 32-1

Scaler control unit.

(3) A millimicrosecond passive delay network. This unit is similar to the one described in the 1960 report[1].

(4) A triple fast coincidence circuit. This unit, which is a transistorized version of a unit described in the 1960 report[1], is under construction.

(5) Power supplies for scintillation counters, for solid state detectors, and for general pulse handling chassis.

(6) Components of the two-dimensional 256-channel analyzer[2]. This system is now being completely transistorized. The analog-to-digital converters, address scalers, address selector system, memory control system, and core drivers have been built and largely debugged. Work is in progress to transistorize the arithmetic scaler and readout system, and to simplify the handling of the counts in the core memory. (L. H. Dunning, H. Fauska, R. E. Karns, Jr., R. A. Matthews, and R. L. McKenzie.)

---

1 Cyclotron Research, University of Washington (1960), p. 43.
2 Cyclotron Research, University of Washington (1961), p. 55; (1960) p. 45; (1959) p. 34; (1957) p. 50.

VIII APPENDIX

33. Statistics of Cyclotron Operation

Principal losses of operating time during the year were caused by: (1) melted contact fingers on the east dee stem shorting assembly; (2) repair and rustproofing of the cyclotron water circulating system heat exchanger. The disposition of the time available for cyclotron operation during the year is given in Tables 33-1, 33-2, and 33-3 which are self-explanatory.

Table 33-1 Division of Cyclotron Time Among Activities

Activity	Time	
	Hours	Per Cent
Normal Operation	5467	79.5
Setup of Experiments	485	7.1
Cyclotron Testing	69	1.0
Scheduled Repairs and Modifications	251	3.6
Unscheduled Repairs	337	4.9
Failure of Experimental Equipment	93	1.4
Unsatisfactory Cyclotron Operation	48	0.7
Experiments Using No Beam	15	0.2
Unrequested Time	104	1.5
Visitors	8	0.1
	6877	100.0

Table 33-2 Division of Normal Operation Time Among Major Facilities

	Time	
	Hours	Per Cent
60-Inch Scattering Chamber	4746	86.8
Target Box Bombardment by Laboratory Personnel	689	12.6
Target Box Bombardment for Others	12	0.2
Tests	21	0.4
	5467	100.0
24-Inch Scattering Chamber Used with No Beam simultaneously with other facilities	168	

Table 33-3 Division of Normal Operation Time Among Projectiles

Projectile	Time	
	Hours	Per Cent
Alpha Particles	4278	78.2
Protons	1141	20.9
Deuterons	48	0.9
	5467	100.0

34. Bombardment for Outside Investigators

During the year bombardments were requested by and performed for a number of outside investigators. These are summarized in Table 34-1.

Table 34-1. Bombardment for Outside Investigators

Investigator	Time	
	Hours	Per Cent
Boeing Airplane Company	1.2	10.3
University of Colorado	3.5	30.0
Western Washington College of Education	7.0	59.7
	11.7	100.0

35. Advanced Degrees Granted, Academic Year 1961-62

Werner M. Brandenberg: M.S.

Charles R. Gruhn: Ph.D. A Study of Particle Emission from a Rotating Nucleus.

Paul H. Gudiksen: M.S.

Charles O. Hower: Ph.D. The (α, Be^7) Reaction in Light Elements at Energies Below 42 Mev.

Joseph E. Ramus: M.S.

Chris D. Zafiratos: Ph.D. A Study of Two Nucleon Stripping and Two Nucleon Pick-Up Reactions in Light Nuclei.

36. Cyclatron Personnel, 1961-62

Faculty

Peter Axel, Visiting Professor[1]
David Bodansky, Associate Professor
Arthur W. Fairhall, Associate Professor
George W. Farwell, Professor
James B. Gerhart, Associate Professor
I. Halpern, Professor
Fred H. Schmidt, Professor
John F. Streib, Associate Professor

Cyclotron Research Staff

Ronald E. Brown, Research Assistant Professor
David K. McDaniels, Research Instructor[2]
Taku Matsuo, Research Instructor[3]
Ted J. Morgan, Research Associate Professor; Supervisor, Cyclotron Laboratory

Graduate Student Pre-Doctoral Associates

Francis Bartis
Joseph Coleman
Darrell M. Drake
Charles R. Gruhn[4]
Isam Naqib
E. Roland Parkinson
Richard W. West
Chris Zafiratos

Graduate Student Research Assistants

Physics

Nelson S. Gillis[5]
Joseph S. Heagney
David L. Hendrie
Wojciech A. Kolasinski
Paul Mizera
Joseph E. Ramus
David C. Shreve
G. S. Sidhu
Frederick W. Slee

Chemistry

Paul Gudiksen[6]
Charles O. Hower[7]
R. L. Watters[8]

Full-Time Technical Staff

Machine Shop

Harvey E. Bennett, Foreman
Norman E. Gilbertson
Charles E. Hart
Floyd E. Helton
Gustav E. Johnson
Bernard Miller, Assistant Foreman
Byron A. Scott
Allen L. Willman

Electronic and Electrical

Lavern H. Dunning
Robert B. Elliott
Harold Fauska, Senior Physicist; Research Electronics Supervisor
Russell E. Karns, Jr.
Richard A. Matthews
Robert L. McKenzie
John W. Orth, Assistant Supervisor, Cyclotron Laboratory
John Turneaure[6]

Design and Drafting

Gerald B. Bartley
Robert G. Clarke
Peggy Douglass
Ralph Flaaten, Engineer[6]
Clyde Louk[6]
James L. Miles
Peter Momcilovich, Engineer
Lewis E. Page

Cyclotron Operators

Barbara J. Barrett
Donna M. Brown[6]
Georgia Jo Rohrbaugh

Others

Patricia A. Kelsh, Radiochemist[6]
Kyum-Ha Lee, Film Scanner
Ann E. Rutter, Secretary
Harriet M. Wasserman, Radiochemist

Part-Time Technical Staff

Student Helpers

Ralph Christofferson
Thomas Hayward
Carol Lewis
Claudelle Pazer
John Rancour
Patricia Rice
Tamae Sato
Akiko Yamanouchi

Others

Sharon A. Gill, Clerk-Typist[6]
Gloria S. Marks, Clerk-Typist
Don A. Miller, Stores Manager
Wm. V. Stolcis, Stores Manager[6]

---

1 Summer, 1961.
2 Now at Centre d'Etudes Nucleaires de Saclay, Gif-sur-Yvette, Seine et Oise, France.
3 Now at Kyushu University, Fukuoka, Japan.
4 Now at Massachusetts Institute of Technology, Cambridge, Massachusetts.
5 Employed during summer only.
6 Terminated.
7 Now at Princeton University, Princeton, New Jersey.
8 O.R.I.N.S. Fellow.

37. List of Publications

The following articles, originating in this laboratory, were published during the year ending June 15, 1962:

"Evaporation of Coincident Protons in α + Ni^{58} Reactions," D. Bodansky, R. K. Cole, W. G. Cross, C. R. Gruhn, and I. Halpern, Phys. Rev. 126, 1082 (1962).

"The Radiochemistry of Magnesium," A. W. Fairhall, National Academy of Sciences--National Research Council, Nuclear Science Series, No. 3024 (1961).

"The Use of Oxygen-14 in the Study of Position Polarization in a Fermi-Type Transition," F. H. Schmidt, J. B. Gerhart, J. C. Hopkins, H. Bichsel, and J. E. Stroth, Radio-isotopes in The Physical Sciences and Industry, pp. 303-12, International Atomic Energy Agency, Vienna (1962).

"Proton Angular Distributions for (α,p) Reactions on C^{12}, Al^{27}, and P^{31}," A. J. Lieber, F. H. Schmidt, and J. B. Gerhart, Phys. Rev. 126, 1496 (1962).

"A Cyclotron Dee Voltage Regulator," J. W. Orth, Cathode Press, 18, 31 (1961).

"Systematics of Octupole States in Nuclei," G. W. Farwell, Proceedings of the Rutherford Jubilee International Conference (Heywood and Company, Ltd., London, 1962), p. 321.

"Magnetic Analysis of 42-Mev Cyclotron Alpha Particles," D. K. McDaniels, W. B. Brandenberg, G. W. Farwell, and D. L. Hendrie, Nuclear Instruments and Methods 14, 263 (1961).

The following abstracts, originating in this laboratory, were published during the year ending June 15, 1962:

"Proton Spin Flip in Inelastic Scattering from C^{12}," F. H. Schmidt, J. B. Gerhart, and W. A. Kolasinsky, Bull. Am. Phys. Soc. 7, 60 (1962).

"C^{12*} Spin Substate Amplitudes in C^{12} (p,p'γ) Scattering at 10.5 Mev," J. B. Gerhart, F. H. Schmidt, W. A. Kolasinsky, and R. E. Brown, Bull. Am. Phys. Soc. 7, 270 (1962).

"Symmetry Axis Behaviour of α - γ Correlations in C^{12} (α,α'γ) Reactions," D. L. Hendrie and D. K. McDaniels, Bull, Am. Phys. Soc. 7, 270 (1962).

"Elastic and Inelastic Scattering of 42-Mev Alphas by Mg^{24}, Al^{27}, and C^{12}," Isam M. Naqib, Bull. Am. Phys. Soc. 7, 73 (1962).